UV Raman Spatially Resolved Melting Dynamics of Isotopically Labeled Polyalanyl Peptide: Slow α-Helix Melting Follows 3_{10}-Helices and π-Bulges Premelting

Aleksandr V. Mikhonin, Sanford A. Asher,* Sergei V. Bykov, and Adrian Murza

Department of Chemistry, University of Pittsburgh, Pittsburgh, Pennsylvania 15260

Received: August 21, 2006; In Final Form: January 12, 2007

We used UV resonance Raman (UVRR) to examine the spatial dependence of the T-jump secondary structure relaxation of an isotopically labeled 21-residue mainly Ala peptide, AdP. The AdP penultimate Ala residues were perdeuterated, leaving the central residues hydrogenated, to allow separate monitoring of melting of the middle versus the end peptide bonds. For 5 to 30 °C T-jumps, the central peptide bonds show a ∼2-fold slower relaxation time (189 ± 31 ns) than do the exterior peptide bonds (97 ± 15 ns). In contrast, for a 20 to 40 °C T-jump, the central peptide bond relaxation appears to be faster (56 ± 6 ns) than that of the penultimate peptide bonds (131 ± 46 ns). We show that, if the data are modeled as a two-state transition, we find that only exterior peptide bonds show anti-Arrhenius folding behavior; the middle peptide bonds show both normal Arrhenius-like folding and unfolding. This anti-Arrhenius behavior results from the involvement of π-bulges/helices and 3_{10}-helix states in the melting. The unusual temperature dependence of the (un)folding rates of the interior and exterior peptide bonds is due to the different relative (un)folding rates of 3_{10}-helices, α-helices, and π-bulges/helices. Pure α-helix unfolding rates are ∼12-fold slower (∼1 μs) than that of π-bulges and 3_{10}-helices. In addition, we also find that the α-helix is most stable at the AdP N-terminus where eight consecutive Ala occur, whereas the three hydrophilic Arg located in the middle and at the C-terminus destabilize the α-helix in these regions and induce defects such as π-bulges and 3_{10}-helices.

Introduction

The classical picture of α-helix melting envisions an elementary process whereby individual peptide bonds at the ends of the α-helix rotate from conformations with α-helical Ramachandran Ψ and Φ dihedral angles to random coil conformations with uncorrelated, but allowed Ramachandran Ψ and Φ dihedral angles.[1−3] This melting also involves breaking the intra-α-helical hydrogen bonds. This highly simplistic view is the basis for the standard theories that are used to model the cooperativity in melting from the α-helix to its melted conformational state(s). This helix ↔ coil transition for short helix-forming peptides has recently been the subject of numerous experimental[4−52] and theoretical[53−116] investigations.

This simple view of α-helix melting is now being challenged, because it appears that simple α-helical peptides in aqueous solutions often melt to predominantly PPII-like conformations,[117−124] which are stabilized mainly by peptide bond−water interactions.[117,125−128] Whether unfolded proteins and peptides exist in "PPII-like" or "random coil" conformations is in active debate in the protein and peptide folding community. However, most recent publications support the existence of PPII-like conformations in proteins[121,129−132] and peptides.[117−124,133−139] Fewer studies support the existence of random coil conformations.[62,140] As pointed out in recent reviews,[125,126,141,142] unfolded peptides and proteins show strong CD signals, which are hard to understand if these unfolded peptides and proteins were truly disordered. In addition, these CD spectra are similar to those found for Polypro. Further, even single peptide bonds of dipeptides in aqueous solution, which were previously expected to be disordered, have recently been found to also show PPII-like spectra.[136,137] Thus, we conclude that there is no convincing evidence in favor of melting to, or even for the existence of, random coil peptides in solution.

Thus, the standard theories for α-helix formation and melting must be modified to include the fact that the transition is not between an ordered α-helix and a disordered random coil conformation, but rather, the transition is between two ordered conformations. Further, this transition must be more complex, because at least one additional interfacial state must occur to connect the α-helix segment to the PPII segment due to the steric features that prevent any simple connection.[68]

Given these complications, it is somewhat surprising that existing theory predicts the α-helix melting behavior pretty well. In most cases, the melting relaxation kinetics appears to follow a single-exponential decay.[4−6,10,13−15,17,18,21,26] It should, however, be noted that clear departures from simple theory to date have been observed, such as an α-helix peptide position dependence for the melting kinetics by Werner et al.'s,[10] Huang et al.'s,[32] and Ramajo et al.'s[25] time-resolved IR isotopically (C═O)-labeled spectral study of the unfolding kinetics of ∼20-residue α-helical peptides. In addition, Huang et al.[32−34] and Bredenbeck et al.[22] found evidence for nonexponential relaxation. Theoretical models have been proposed to explain the observed nonexponential kinetics.[33,63]

We recently used UV resonance Raman (UVRR) spectroscopy[7] to examine the spatial dependence of melting of an isotopically labeled mainly Ala α-helical peptide, AdP. UVRR spectroscopy is a powerful method to quantitatively determine peptide secondary structures.[4,7,135,143−153] UV excitation within the peptide bond $\pi' \rightarrow \pi^*$ transition selectively enhances a number of amide vibrations whose frequencies and intensities report on the polypeptide backbone conformation.[4,135,143−145,154−157]

* Corresponding author. E-mail: asher@pitt.edu. Telephone: (412)-624-8570. Fax: (412)-624-0588.

10.1021/jp0654009 CCC: $37.00 © 2007 American Chemical Society
Published on Web 03/06/2007

The UVRR spectra are highly resolved. Laser induced temperature-jump (T-jump) kinetic UVRR measurements allow detailed studies of peptide unfolding.[4−6] In these studies, the temperature of the peptide aqueous solution is increased within nanoseconds by an IR laser pulse whose wavelength is completely absorbed by a water combination band. The temperature increase initiates peptide unfolding. A subsequent 204 nm UV excitation pulse at the appropriate delay time after the T-jump excites the UVRR spectra.

These UVRR spectra can be used to monitor the relaxation of the peptide conformation. For natural abundance AP, we previously observed[4−6] a simple moderately cooperative melting curve with apparently simple single-exponential relaxation kinetics (∼200 ns). The only indication of complexity in the kinetics came from a two-state analysis of the temperature dependence, which demonstrated an anti-Arrhenius temperature dependence for the α-helix folding rate constant. The relaxation kinetics observed were similar to the melting behaviors observed for similar α-helical polypeptides.[4−6,10,13−15,17,18,21]

In a previous study, we isotopically labeled AP in order to separately monitor the end peptide bonds melting versus that of the interior peptide bonds.[7] We found that the central peptide bonds have a higher equilibrium melting temperature than do the end peptide bonds. In the work here, we directly examine the spatial dependence of unfolding kinetics for this partially deuterated peptide, AdP. As discussed below, we find faster relaxation kinetics for the end peptide bonds compared with the middle for a 5 to 30 °C T-jump. In contrast, we find slower relaxation kinetics for the end peptide bonds compared with the middle for the 20 to 40 °C T-jump. We find that this behavior results from different relative contributions in the different regions of slower melting pure α-helices and faster melting π-bulges and 3_{10}-helices to the observed melting kinetics.

The AdP kinetic data can be adequately fit by single exponentials, within the S/N of our data. However, if we apply a two-state model similar to that of Lednev et al.,[4] we calculate strong anti-Arrhenius behavior for folding of the end peptide bonds, whereas the middle peptide bond (un)folding shows a normal Arrhenius behavior. This apparent anti-Arrhenius behavior results from involvement of additional states. These results are consistent with recent evidence that the ends of AdP-like peptides are frayed.[7,12,23,25,28,29,31,37,43,75,80] We successfully model the observed anti-Arrhenius behavior by taking into account π-bulge and 3_{10}-helical conformation melting, in addition to that of the pure α-helix. This model is supported by recent studies by us and others, which report evidence for 3_{10}-helix[56,72,74,86,158−171] and π-helix/bulge[57,98,166,171−174] conformations in Ala-rich peptides. Further, our model also explains the complicated nonexponential behavior observed earlier by Huang et al.[34] and Bredenbeck et al.[22] for similar peptides.

Materials and Methods

Materials. The partially deuterated 21-residue alanine-based peptide (AdP) as well as its natural abundance analogue AP (also called Fs) were synthesized by AnaSpec. Inc. The eight terminal Ala at the amino end and the six terminal Ala at the carboxyl end of the AdP peptide were perdeuterated while maintaining a non-deuterated center ($\mathbf{A_dA_dA_dA_dA_dA_dA_dA_d}$-RAAAA-R$\mathbf{A_dA_dA_dA_d}$-R$\mathbf{A_dA_d}$, where the bold letters label the 2,3,3,3-deuterated residues).

The AdP purity as well as the position of deuterated amino acid residues was independently verified by MALDI MS analysis kindly performed by Anton Karnoup (The Dow Chemical Company, Midland, MI). Analysis was carried out using a Voyager DE-STR MALDI-TOF mass spectrometer (Applied Biosystems) operated in reflectron and post-source decay (PSD) modes.

T-Jump Raman Spectral Measurements. The UV Raman spectrometer is described in detail elsewhere.[4,175] Briefly, the third harmonic of a Coherent Infinity Nd:YAG laser operating at 90 Hz with a 3 ns pulse width was Raman-shifted five anti-Stokes harmonics in 40 psi hydrogen gas to 204 nm to excite the amide band UVRR spectra. The Raman scattered light was collected at an angle close to backscattering and dispersed with a partially subtractive double monochromator. The Raman scattered light was detected by using a Princeton Instruments Spec-10:400B CCD camera (Roper Scientific). We used spectral accumulation times of ∼5 min with spectral resolutions of ∼10 cm^{-1}.

To selectively heat the water solvent, we Raman-shifted the 1.06 μm Nd:YAG fundamental to 1.9 μm (first H_2 Stokes shift) by using a 1 m Raman shifter (Light Age Inc.; 1000 psi H_2) to obtain 1.5 mJ pulse energies at our 90 Hz repetition rate. This 1.9 μm excitation is absorbed by a water combination band, and the energy is thermalized in picoseconds by vibrational relaxation.

We studied T-jumps from 5 to 30 and from 20 to 40 °C. These T-jumps were obtained by focusing the 1.5 mJ 1.9 μm laser pulses to a ∼300 μm diameter spot in the flowing sample stream. To ensure that the Raman signal was obtained from the sample volume maximally heated by the IR pulse,[4] we adjusted the sample absorbance at 204 nm to 40 cm^{-1} by utilizing a 15 mg/mL concentration of AdP.

We independently verified the magnitude of the T-jump by measuring the pump beam energy dependence of the 204 nm excited ∼3000 cm^{-1} water Raman band. This band shows a large, well-known frequency and band shape temperature dependence.[4,176,177] We constructed a T-jump calibration curve as described by Lednev et al.[4] by using the UVRR water difference spectrum in the presence versus absence of the IR pump beam to determine the actual T-jump in the probed volume.

There exist low temporal frequency variations of the measured Raman spectral intensities that can interfere with the T-jump spectral measurements. These variations may derive from variations in the UV laser pulse energy at the sample. Alternatively, this variation may derive from low-frequency motion of the sample stream, which may correlate with changes in the sample stream surface. We found that we could remove this fluctuation in the spectra by measuring for each time delay two duplicate T-jump spectra that were bracketed by identically measured cold spectra where the T-jump pump pulses were blocked. We only accepted as valid T-jump spectra that were bracketed by essentially identical cold UVRR spectra. This allowed us to ignore the set of fluctuations that did not span the time scale of repeated T-jump measurements.

Uncertainties in the Nonlinear Parameter Estimation. We determined the secondary structure composition from the steady state and transient spectra for the AdP $C_\alpha-H$ peptide bonds in the center and for the $C_\alpha-D$ penultimate amide bonds by fitting the experimentally measured spectra to a linear combination of the four basis spectra of the α-helix and PPII conformations of the $C_\alpha-H$ and $C_\alpha-D$ peptide bonds, as determined earlier.[145] The fits were obtained by using least-squares criteria. In this modeling, we assume that each of the amide groups scatter independently[178] and that the spectra derived from the previously determined basis spectra of the α-helix and PPII conforma-

tions,[4,120,145] taking into account that the PPII basis spectra were previously[4] incorrectly assigned to a "random coil" conformation.

We deconvoluted the 82 °C PPII spectrum of AdP into a minimum number of bands as in Lednev et al.[4] We then determined the temperature dependence of the band intensities, bandwidths, and frequencies in spectra measured of AdP at 52, 62, 70, and 82 °C, temperatures at which AP and, thus, AdP is predominantly PPII.[4,6,120] We assumed that this observed linear temperature dependence extrapolates down to 0 °C and calculated the pure temperature-dependent PPII spectra of AdP. Because the individual PPII peptide bonds independently contribute to the UVRR spectra,[178] the AdP PPII spectra have a 35% contribution from the $C_\alpha-H$ PPII peptide bonds (7 out of 20 bonds) and a 65% contribution from the $C_\alpha-D$ PPII peptide bonds (13 out of 20 bonds). We subtracted the necessary amount of the temperature-dependent $C_\alpha-H$ AP PPII spectra from the AdP PPII spectra to uniquely calculate the temperature-dependent $C_\alpha-D$ AdP PPII spectra.

We know that AdP is ~53% α-helix-like at 5 °C.[4,6,7,171] Because AdP contains 35% $C_\alpha-H$ peptide bonds and 65% $C_\alpha-D$ peptide bonds and the $C_\alpha-H$ b Raman band derives only from the $C_\alpha-H$ peptide bond PPII Raman spectrum,[4,144,145,154] we can determine the $C_\alpha-H$ PPII fraction at 5 °C directly from the $C_\alpha-H$ b band intensity. This $C_\alpha-H$ PPII fraction knowledge allows us to directly estimate the $C_\alpha-D$ PPII and $C_\alpha-H$ α-helix-like fractional compositions. We can also calculate the pure $C_\alpha-D$ peptide bond α-helix-like basis spectrum by subtracting the calculated 5 °C $C_\alpha-D$ peptide bond PPII spectrum, as well as the calculated 5 °C $C_\alpha-H$ peptide bond PPII and α-helix spectra from the measured 5 °C AdP spectrum. We assume that this α-helix-like basis spectrum is independent of temperature.[4,179]

We estimated the errors in our secondary structure determinations by calculating the Jacobian matrix as we iterate to the best fit solutions.[180−182] To relate the parameter standard error to the experimental error and to the Jacobian matrix we make the following assumptions: The measured spectral data are assumed to have the form

$$y_{i,j} = f(x_i;p_1,p_2,...) + \epsilon_i \tag{1}$$

where the errors ϵ_i are assumed to be normally distributed random values with standard deviation, σ_i. The second assumption is that the true noiseless spectrum $f(x_i;p_1,p_2,...)$ can be exactly modeled as for the specific set of j parameters ($p_1,p_2,...,p_j$). Under these assumptions, we express an uncertainty bound for each individual parameter using information obtained from the variance−covariance matrix c, which is approximated by the Jacobian matrix[181−183] evaluated at the sum of squares minimum values p^*, which give rise to the best spectral fit $f(x_i;p_1^*,p_2^*,...)$. Thus,

$$c(p^*) = C^{-1}(p^*) = [J^T(p^*)\,J(p^*)]^{-1} \tag{2}$$

where J is the Jacobian

$$J_{i,j} = \partial f(x_i;p_1,p_2,...)/\partial p_j \tag{3}$$

Equation 2 implies the additional assumptions: (1) that the optimal function $f(x_i;p_1^*,p_2^*,...)$ is well approximated by a multidimensional Taylor expansion around the minimum, which includes the curvature matrix $C(p^*)$ in its second-order term and (2) that $C(p^*)$ is, in turn, well approximated by the product $J^T(p^*)\,J(p^*)$.[182,183]

The estimated standard error of the parameter p_j is

$$\sigma_j = (c_{jj}\chi^2)^{1/2} \tag{4}$$

where c_{jj} refers to the diagonal element of the variance−covariance matrix and χ^2 is the reduced chi-squared statistical parameter.[180−183] χ^2 is calculated as

$$\chi^2 = \frac{\sum_{i=0}^{n}[y_i - f(x_i;p_1,p_2,...)]^2}{\mathrm{DOF}} \tag{5}$$

where DOF is the degrees of freedom, DOF = n - j, as previously described.[184]

Weighting the Least-Squares Fit. We performed weighted least-squares fitting of the resulting calculated time-dependent AdP $C_\alpha-H$ peptide bond and $C_\alpha-D$ peptide bond PPII concentrations to single-exponential functions to determine relaxation rates for the center and penultimate peptide bonds. The weighted sum of squares to be minimized was evaluated as[185]

$$\chi^2 = \frac{\sum_{i=0}^{n} w_i[t_i - f(x_i;p_1,p_2,...)]^2}{\sum_{i=0}^{n} w_i} \tag{6}$$

where the weights w_i are calculated from the estimated variances ϱ_i^2 in the fractions of AdP $C_\alpha-H$ peptide bond and $C_\alpha-D$ peptide bond PPII concentrations:

$$w_i = (1/\varrho_i)^2 \tag{7}$$

and t is the kinetic delay time after the T-jump. Equation 4 estimates the standard error of the calculated parameter. The reduced χ^2 was obtained as

$$\chi^2 = \frac{\sum_{i=0}^{n} w_i[y_i - f(t_i;p_1,p_2,...)]^2}{\mathrm{DOF}\sum_{i=0}^{n} w_i} \tag{8}$$

Results

AdP UV Resonance Raman Spectra. Figure 1 shows the 5 °C 204 nm excited UVRR spectra of aqueous solutions of the 21 amino acid residue peptides AdP and AP, where AP is the natural abundance analogue of AdP. At 5 °C, AdP and AP are ~53% α-helix-like and ~47% PPII.[4,6,7,120,171] We previously calculated the UVRR spectra of the individual α-helix-like and PPII conformations.[7,145] Most recently, we showed that the 5 °C α-helix-like conformations actually consist of ~24% pure α-helix, ~20% π-bulges/helices, and ~9% 3_{10}-helices whose spectra overlap (see below).[171]

As discussed in detail elsewhere,[145,171] α-helix-like AP conformations display a triplet of bands in the amide III region. The 1261 cm^{-1} $AmIII_{3H}$ band was originally[145] assigned to the "classical α-helix AmIII band" and involves mainly N−H b, C−N s, and possibly $C_\alpha-C$ s. However, we recently showed

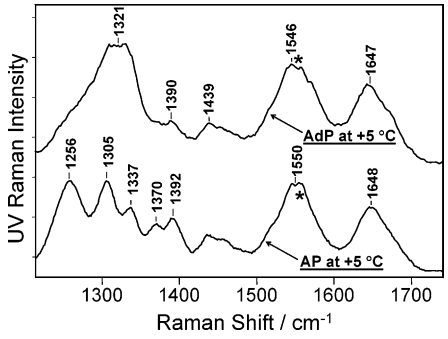

Figure 1. 204 nm UV Resonance Raman spectra of AdP (15 mg/mL) and its natural abundance analogue AP (3 mg/mL) at 5 °C. The AP solution contained 0.2 M $NaClO_4$. The star marks an overlapping molecular oxygen stretching band.

that this $AmIII_{3H}$ band has contributions not only from pure α-helix conformations but also from overlapping bands due to π-bulges and 3_{10}-helices at $T < 30$ °C, which broaden the $AmIII_{3H}$ band.[171] The 1306 cm^{-1} band was assigned to the $AmIII_2$ vibration, which mainly involves $C_\alpha-C$ s, N−C s, with possibly a small amount of C−N s and N−H b,[145] and the 1337 cm^{-1} band was assigned to the $AmIII_1$ band, which derives from a vibration mainly involving $C_\alpha-C$ s and N−C s, with possibly a small amount of C−N s.[145] The α-helix-like AmII band, which occurs at 1542 cm^{-1}, is mainly associated with C−N s and N−H ib, and the 1647 cm^{-1} α-helix-like Am I band involves mainly C═O s.[145,186]

We demonstrated earlier[145] that the AmIII band triplet of the AP PPII conformation occurs at 1245 ($AmIII_3$), 1303 ($AmIII_2$), and 1337 cm^{-1} ($AmIII_1$), with the 1245 cm^{-1} band labeled as the "classical AmIII band". The PPII conformation of AP also shows a doublet at 1370 and 1394 cm^{-1}, which mainly derives from $C_\alpha-H$ b with maybe some contribution from CH_3 umbrella modes. These $C_\alpha-H$ bands are absent in the α-helix conformation.[4,144,145,154,187]

The AP PPII conformation AmII and AmI bands are upshifted and broadened compared to those of the α-helix-like conformations.[4,145] AmII appears at 1558 cm^{-1}, and AmI appears at 1655 cm^{-1} in the PPII conformation. There are also relatively broad Arg side chain bands, one of which occurs at ∼1646 cm^{-1} in water and overlaps the AP AmI band.[178] In contrast, this Arg band in D_2O is much sharper and occurs at ∼1614 cm^{-1}, well separated from the AmI band.[178]

The AdP UVRR spectra are much more complex because of contributions from both $C_\alpha-H$ and $C_\alpha-D$ peptide bonds, which occur in both α-helix-like and PPII conformations. Mikhonin and Asher[178] recently demonstrated that the peptide amide III−$C_\alpha-H$ bands region in the UVRR spectra result from the independent UVRR contributions of the different peptide bonds. Thus, the spectra of AdP can be considered to result from independent scattering from $C_\alpha-H$ and $C_\alpha-D$ peptide bonds in α-helix-like and PPII conformations.

The $C_\alpha-D$ peptide bonds show UVRR spectra[144,145] that differ from those of natural abundance AP mainly in an upshift of the $C_\alpha-D$ peptide bond amide III band envelope to ∼1321 cm^{-1}. In AdP, the 1321 cm^{-1} band dominates the amide III spectral region (Figure 1). Deuteration of the Ala residue $C_\alpha-H$ decouples the NH bend from the $C_\alpha-H$ bending motion.[144] The resulting $C_\alpha-D$ amide III band no longer shows a triplet but displays a complex band shape with an increased Raman cross section.[7,144,145] The loss of $C_\alpha-H$ bending coupling leaves this band frequency insensitive to the peptide bond conformational difference between the α-helix and PPII conformations.[7,144,145] However, the Raman cross section of this band is much larger

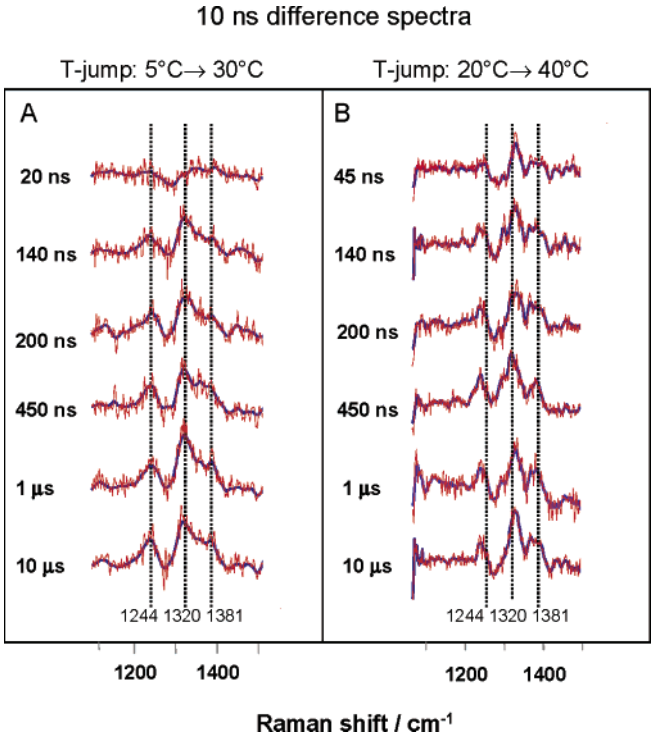

Figure 2. T-jump difference UVRR spectra of AdP at different delay times between the pump and probe laser pulses. These difference spectra were obtained by subtracting the 10 ns delay time spectra from each of the longer delay time spectra. (A) Difference spectra for a T-jump from 5 to 30 °C. (B) Difference spectra for a T-jump from 20 to 40 °C.

for the PPII conformation[145] due to the hypochromism present in the α-helix conformation.[188−197]

Although the $C_\alpha-H$ Ala CH_3 side chain umbrella bending vibration contributes to the 1370−1400 cm^{-1} spectral region,[186] the intensity in this region is dominated by the resonantly enhanced $C_\alpha-H$ b doublet of the $C_\alpha-H$ Ala PPII conformation.[120,145] Thus, changes in PPII concentration dominate the intensity changes within this spectral region. Furthermore, the CH_3 umbrella UVRR bands are expected to be insensitive to conformational changes in the peptide backbone, as shown recently.[145]

Transient AdP UVRR Difference Spectra. Figure 2 shows a series of calculated UVRR difference spectra measured at different delay times subsequent to a T-jump. The raw spectra were obtained by measuring UVRR spectra at specified delay times after the T-jump. The time delay difference spectra shown in Figure 2 were calculated by subtracting a spectrum measured 10 ns after the T-jump from the individual time delayed spectra. We utilized T-jumps that increased the sample temperature from 5 to 30 and from 20 to 40 °C.

We subtracted the 10 ns delay spectra from the original T-jump difference spectra to selectively remove spectral changes that derive from sample non-conformational temperature changes.[4−6,120] We earlier showed that these non-conformational changes derive from a decreased hydrogen bond strength to water at elevated temperatures.[4,6,120,135,145] This allows us to concentrate on spectral alterations induced by conformational changes, which occur at later times. Our previous AP studies[4−6,120] clearly showed that no conformational changes occur until longer (>50 ns) delay times.

The main Figure 2 UVRR difference features occur as bands at 1320 and 1381 cm^{-1} whose intensities increase with the time delay after the T-jump. The 1320 cm^{-1} feature derives from an

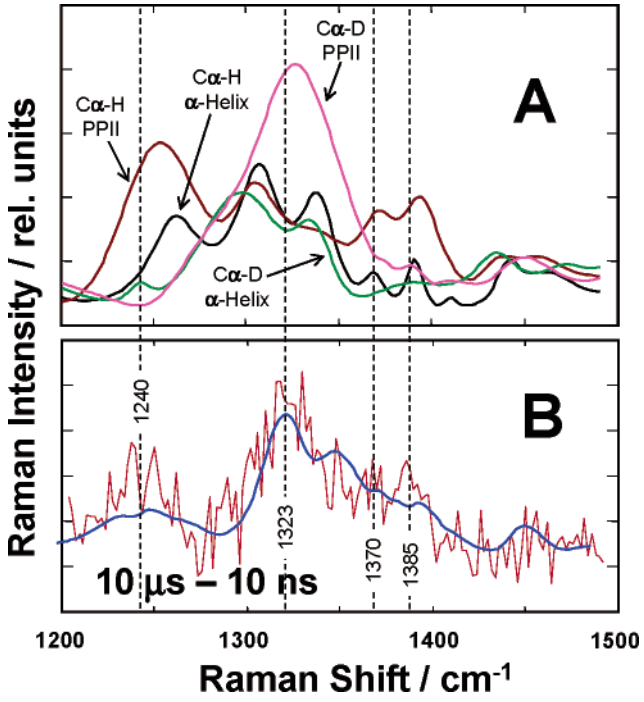

Figure 3. (A) Calculated 30 °C pure secondary structure spectra of AdP: $C_\alpha-H$ peptide bond α-helix-like conformation (black); $C_\alpha-H$ peptide bond PPII conformation (brown); $C_\alpha-D$ peptide bond α-helix-like conformation (green); and $C_\alpha-D$ peptide bond PPII conformation (magenta). (B) Measured transient difference spectrum obtained after a time delay of 10 μs during a T-jump from 5 to 30 °C (red); also shown is a best fit of AmIII−C_α−H region (1200−1480 cm^{-1}) to a linear combination of the AdP basis spectra shown in Figure 5A (blue).

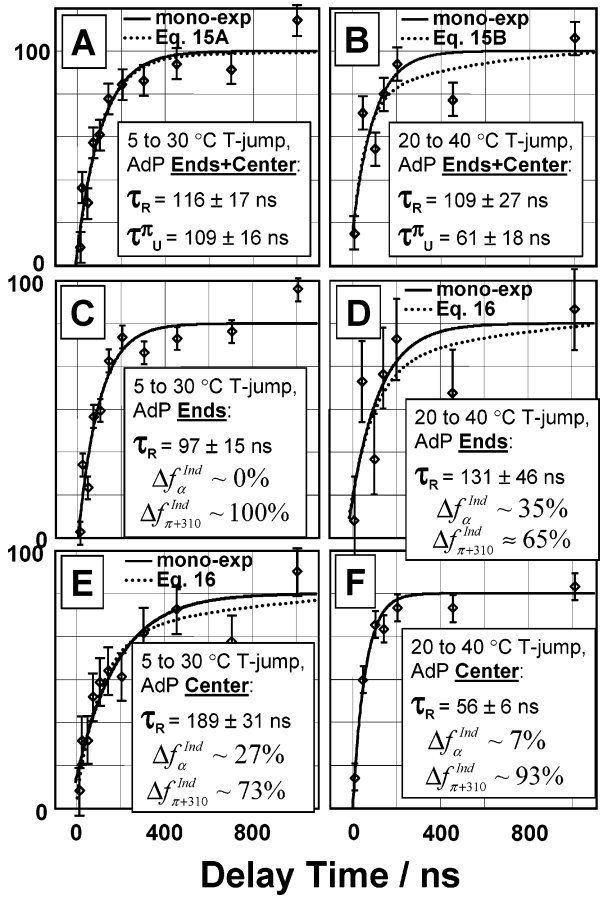

Figure 4. T-jump relaxation of the total PPII concentration (A and B) as well as the PPII concentrations of the end $C_\alpha-D$ (C and D) and center peptide bonds (E and F) due to T-jumps from 5 to 30 and 20 to 40 °C. Unfolding is monitored by changes in the relative compositions of the basis spectra shown in Figure 3. The monoexponential relaxation times are $\tau_{total} = 114 \pm 46$, $\tau_{end} = 89 \pm 17$, and $\tau_{cen} = 188 \pm 46$ ns for the T-jump from 5 to 30 °C and $\tau_{total} = 96 \pm 39$, $\tau_{end} = 122 \pm 51$, and $\tau_{cen} = 54 \pm 11$ ns for the T-jump from 20 to 40 °C. The dotted lines in Figure 4A, B are fits to the eq 15 kinetics for the total PPII concentrations. These fits find the unfolding times, τ_U^π, for π-bulges (or 3_{10}-helices) of 109 ± 24 ns for the 5 to 30 °C T-jump and 61 ± 23 ns for the 20 to 40 °C T-jump.

AmIII band intensity increase from the $C_\alpha-D$ peptide bonds of AdP due to the increasing PPII concentration. Melting to the PPII conformation results in hyperchromism[188−197] of the resonant absorption band and a consequent hyperchromism of the Raman cross sections.[145] The 1381 cm^{-1} intensity increase results from the appearance of the $C_\alpha-H$ b band of the AdP melted $C_\alpha-H$ PPII conformation.[120]

Modeling the Transient Temperature Dependence of AdP Secondary Structure. We used the calculated AP and AdP pure secondary structure-Raman spectra (PSSRS) to determine the time delay-dependent secondary structure composition for each observed transient AdP UVRR spectrum at each T-jump. Figure 3A shows the calculated temperature-dependent PPII $C_\alpha-H$ peptide bond and $C_\alpha-D$ peptide bond basis spectra and the temperature-independent α-helix $C_\alpha-H$ peptide bond and $C_\alpha-D$ peptide bond basis spectra.[4,145]

We did not attempt to resolve the underlying pure α-helix, π-helix/bulge, and 3_{10}-helix conformations recently discovered by Mikonin and Asher[171] in these transient spectra given our limited S/N. The affect of their contribution is to broaden the $C_\alpha-H$ peptide bond "α-helix-like" $AmIII_3$ band.[171]

We can precisely determine AdP PPII fractions for the $C_\alpha-H$ peptide bonds using the basis spectra, because the $C_\alpha-H$ b band(s) between 1380 and 1400 cm^{-1} (Figure 4A) serves as an isolated, extremely sensitive non-α-helical marker.[4,144,145,154] For the $C_\alpha-D$ peptide bonds, $C_\alpha-D$ deuteration breaks the coupling between the $C_\alpha-D$ b and N−H b motions, which makes the $C_\alpha-D$ AmIII band frequency insensitive to the Ψ Ramachandran angle.[144,145] However, it is still possible to reliably find the $C_\alpha-D$ PPII fraction by using the normalized basis spectra, because the intensity of the $C_\alpha-D$ PPII AmIII band is more than 2-fold greater than that of the $C_\alpha-D$ "α-helix-like" AmIII band (Figure 3A)[145] due to hypochromic excitonic interactions in the α-helix.[188−197] Using this approach, we can reliably estimate the PPII fractional compositions in AdP $C_\alpha-H$ center peptide bonds as well as in the $C_\alpha-D$ end peptide bonds from the different transient spectra shown in Figure 2 at different delay times, *t*, subsequent to T-jumps from 5 to 30 and 20 to 40 °C.

AdP Monoexponential Relaxation Rates. Figure 4A, B shows the time dependence of the calculated total PPII concentration of AdP, as well as the individual end $C_\alpha-D$ PPII and the center $C_\alpha-H$ PPII concentrations for the T-jumps from 5 to 30 and 20 to 40 °C, respectively. Using monoexponential fitting for total PPII concentration ($C_\alpha-D$ plus $C_\alpha-H$ peptide bonds), we find the relaxation time ($\tau_R = k_R^{-1}$) of 116 ± 17 ns (Figure 4A, Table 1) for the T-jump from 5 to 30 °C, whereas for the T-jump from 20 to 40 °C we find a 109 ± 27 ns relaxation time (Figure 4B, Table 1). These relaxation times are identical (within the experimental error) to that found earlier by Lednev et al.[4] for the AP peptide, the natural abundance analogue of AdP. Specifically, Lednev et al.[4] found 180 ± 60, 120 ± 50, and 70 ± 30 ns relaxation times for T-jumps from 4 to 37 °C, from 4 to 48 °C, and from 4 to 64 °C, respectively.

TABLE 1: Two-State Kinetic Parameters and Equilibrium Constant for α-Helix ↔ PPII Conformational Transition Calculated for AdP $C_\alpha-H$ Center, Adp $C_\alpha-D$ End, and All Adp $C_\alpha-H + C_\alpha-D$ Peptide Bonds

	final T-jump temperature ° C		activation energy, ΔG kcal/mol PB
	+30 °C	+40 °C	
relaxation time, $\tau_R = (k_R)^{-1}$/ns			
$C_\alpha-H + C_\alpha-D$	116 ± 17 ns	109 ± 27 ns	1.0 ± 5.5
$C_\alpha-H$ center	189 ± 31 ns	56 ± 6 ns	22.8 ± 3.6
$C_\alpha-D$ ends	97 ± 15 ns	131 ± 46 ns	−5.6 ± 7.3
equilibrium constant,[a] $K^{EQ} = f_{PPII}/f_\alpha$			
$C_\alpha-H + C_\alpha-D$	3.35	5.25	
$C_\alpha-H$ center	0.75	2.03	
$C_\alpha-D$ ends	9.0	19.0	
unfolding time constant, $\tau_U = (k_U)^{-1}$/ns			
$C_\alpha-H + C_\alpha-D$	150 ± 28 ns	130 ± 39 ns	2.7 ± 6.5
$C_\alpha-H$ center	440 ± 100 ns	84 ± 11 ns	31.2 ± 4.9
$C_\alpha-D$ ends	108 ± 19 ns	138 ± 51 ns	−4.6 ± 7.7
folding time constant, $\tau_F = (k_F)^{-1}$/ns			
$C_\alpha-H + C_\alpha-D$	502 ± 91 ns	684 ± 202 ns	−5.8 ± 6.5
$C_\alpha-H$ center	332 ± 75 ns	164 ± 21 ns	13.3 ± 4.9
$C_\alpha-D$ ends	971 ± 167 ns	2620 ± 970 ns	−18.7 ± 7.7

[a] Equilibrium constant between α-helix-like and PPII conformations (see text for detail).

As pointed out by Lednev et al.,[4] if the α-helix melting in AdP were truly a two-state transition, the α-helix folding, k_F, and unfolding, k_U, rate constants could be simply calculated from the "two-state" relaxation rate constant relationship $k_R = k_U + k_F$ and from the two-state equilibrium constant $K_{EQ} = k_U/k_F$ independently obtained from the measured equilibrium UVRR spectra.[4,7] If we use the two-state model, then the $C_\alpha-H$ center (un)folding rate constant shows a "normal" Arrhenius behavior. In contrast, the $C_\alpha-D$ ends folding rate constant decreases with increasing temperature. This is an apparent anti-Arrhenius behavior (with a negative folding activation barrier). As expected, the end peptide bonds melt at lower temperatures than do the middle peptide bonds.[7] However, our kinetic results are quite unusual. For the 5 to 30 °C, we calculate a 2-fold faster relaxation time for the end peptide bonds (97 ± 15 ns, Figure 4C) than that of the middle (189 ± 31 ns, Figure 4E). In contrast, for the 20 to 40 °C T-jump, we calculate a somewhat slower relaxation time for the end peptide bonds (131 ± 46 ns, Figure 4D) than the middle (56 ± 6 ns, Figure 4F).

If these data are modeled as if they result from a two-state transition, we find that the folding rate constants for the AdP end peptide bonds show the strong anti-Arrhenius behavior with a negative activation energy barrier (Table 1). In contrast, we find that all the (un)folding rate constants for the AdP center peptide bonds show the normal Arrhenius-like behavior with positive activation energy barriers (Table 1).

The anti-Arrhenius behavior of AdP ends folding rate constants indicates that the AdP ends melting is clearly not a two-state state process and that the additional states must be involved in the α-helix melting. This is consistent with the recent reports that indicate that the ends of AP and AdP-like peptides are frayed.[7,12,23,25,28,29,31,37,43,75,80]

In contrast, the normal Arrhenius-like behavior of AdP center (un)folding rate constants, at first glance, could indicate that the AdP center melting occurs in "two-state-like" mechanism. However, the Table 1 calculated "two-state" activation energy barriers of ∼10−35 kcal/mol peptide bond (kcal/mol PB) are much higher than those of ∼2−4 kcal/mol PB estimated earlier for Ala-rich peptides both theoretically[56,89,93] and experimentally.[171]

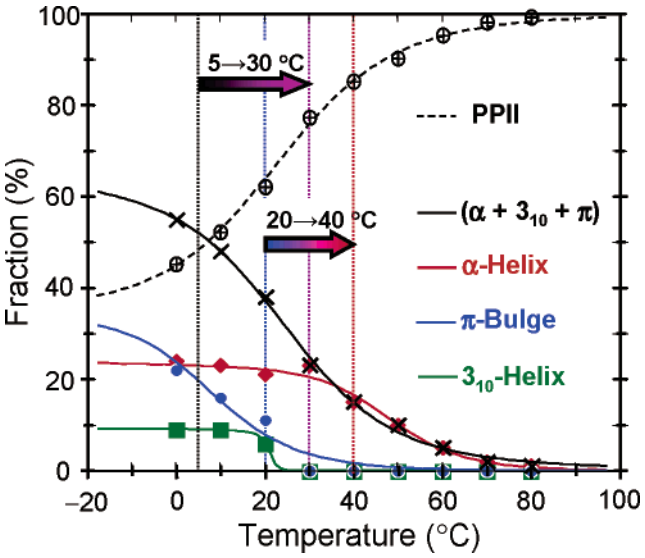

Figure 5. Melting/formation curves for AdP "α-helix-like" conformations. (×) Original "α-helix" melting curve as reported for the natural abundance analogue of AdP, AP, by Lednev et al.,[4,6] which is actually the sum of the individual α-, π-, and 3_{10}-helical melting curves. (red ♦) Pure α-helix melting. (green ■) 3_{10}-Helix (type III turn) melting. (blue ●) π-Bulge (π-helix) melting. (⊕) PPII formation. Arrows show the conformational differences spanned by the 5 to 30 and 20 to 40 °C T-jumps. Adapted from ref 171.

TABLE 2: Total Equilibrium Concentrations of AdP α-Helix-Like Conformations (Including Both $C_\alpha-H$ and $C_\alpha-D$ Peptide Bonds) at Initial and Final T-jump Temperatures

temperature °C	α-helix fraction[a] %	π-helix/bulge fraction[a] %	3_{10}-helix fraction[a] %	total α-helix-like fraction[b] %
+5	24	20	9	53
+30	23	0	0	23
	$\Delta f_\alpha = 1$	$\Delta f_\pi = 20$	$\Delta f_{310} = 9$	$\Delta f_{\alpha+\pi+310} = 30$
+20	22	11	6	39
+40	15	0	0	15
	$\Delta f_\alpha = 7$	$\Delta f_\pi = 11$	$\Delta f_{310} = 6$	$\Delta f_{\alpha+\pi+310} = 24$

[a] We assume that AdP contains the same fractions of α-helix-like conformations as its natural abundance analogue, AP.[171] [b] As was originally reported by Lednev et al.,[4,6] because it was not possible at that time to discriminate between the different α-helix-like conformations.

Below, we explain the unusual kinetic behaviors of both AdP ends and the AdP center in terms of competition between the slower melting pure α-helices and faster melting π-bulges and 3_{10}-helices.

Discussion

We show that this apparent anti-Arrhenius behavior (Table 1) is the result of the failure of the two-state model to describe both the conformational equilibrium and the dynamics of AP or AdP melting. As shown, we can model the observed melting behavior by including the melting of 3_{10}-helical and π-bulge conformational states,[171] in addition to that of the pure α-helix (Figure 5 and Table 2). This modeling explains the observed apparent anti-Arrhenius behavior (Table 1). The individual (un)-folding rate constants for pure α-helices, π-bulges and 3_{10}-helices show normal Arrhenius behavior (Table 3).

TABLE 3: Kinetic Parameters for AdP Pure α-Helix, π-Bulge, and 3_{10}-Helix (Un)Folding, Calculated from the Overall ($C_\alpha-H$ and $C_\alpha-D$ Peptide Bonds) Kinetic and Equilibrium Data Using Eq 15, or from the Individual $C_\alpha-H$ Center Peptide Bonds and $C_\alpha-D$ End Peptide Bond Kinetic and Equilibrium Data Using Eq 16

	final T-jump temperature ° C		
	+30 °C	+40 °C	activation energy, ΔG kcal/mol PB
equilibrium constant,[a] $K_{EQ} = f_{PPII}/f_\alpha$			
$C_\alpha-H + C_\alpha-D$	3.35	5.25	
$C_\alpha-H$ center	0.75	2.03	
$C_\alpha-D$ ends	9.0	19.0	
mono-exp relaxation time, $\tau_R = (k_R)^{-1}$/ns			
$C_\alpha-H + C_\alpha-D$	116 ± 17 ns	109 ± 27 ns	1.0 ± 5.5
$C_\alpha-H$ center	189 ± 31 ns	56 ± 6 ns	22.8 ± 3.6
$C_\alpha-D$ ends	97 ± 15 ns	131 ± 46 ns	−5.6 ± 7.3
pure conformation folding time, $\tau_F = (k_F)^{-1}$/ns			
pure α-helix[b]	4421 ± 802 ns	3553 ± 1207 ns	4.1 ± 7.2
π-bulge and/or 3_{10}-helix[b]	$\tau_F \gg 109$ ns	$\tau_F \gg 61$ ns	4.1 ± 7.2[c]
pure conformation unfolding time, $\tau_U = (k_U)^{-1}$/ns			
pure α-helix[b]	1321 ± 239 ns	677 ± 230 ns	12.6 ± 7.2
π-bulge and/or 3_{10}-helix[b]	109 ± 16 ns	61 ± 18 ns	11.0 ± 6.2
pure conformation relaxation time, $(1/\tau_U + 1/\tau_F)^{-1}$/ns			
pure α-helix[b]	1017 ± 148 ns	568 ± 165 ns	11.0 ± 6.2
π-bulge and/or 3_{10}-helix[b]	109 ± 16 ns	61 ± 18 ns	11.0 ± 6.2
relative contributions of slower pure α-helix relaxation to the observed relaxation kinetics, Δf_α/%			
$C_\alpha-H + C_\alpha-D$[b]	5 ± 8%	29 ± 14%	
$C_\alpha-H$ center[d]	27 ± 9%	7 ± 12%	
$C_\alpha-D$ ends[d]	−3 ± 9%	35 ± 22%	
relative contributions of faster π-bulges and 3_{10}-helix relaxations to the observed relaxation kinetics, $\Delta f_{\pi+310}$/%			
$C_\alpha-H + C_\alpha-D$[b]	95 ± 8%	69 ± 14%	
$C_\alpha-H$ center[d]	73 ± 9%	93 ± 12%	
$C_\alpha-D$ ends[d]	103 ± 9%	65 ± 22%	

[a] These data are identical to those in Table 1. However, here, we recognize that for T ≥ +30 °C the equilibrium includes only the pure α-helix and the PPII conformations[171] (see text for detail). Data from Ianoul et al.[7] [b] We calculated these parameters from the overall ($C_\alpha-H$ and $C_\alpha-D$ peptide bond) kinetic data using eqs 15A and 15B and the equilibrium data summarized in Table 2 (see text for detail). [c] We assume that the activation energy barriers for both the π-bulge and 3_{10}-helix formation (folding) are equal to that of the pure α-helix, because formation of α-helix, π-bulge, and 3_{10}-helix conformations should start from the same (presumably PPII) basin and pass through the same intermediate "turn" region of the Ramachandran plot. [d] We calculated these parameters from the individual $C_\alpha-H$ center and $C_\alpha-D$ end peptide bond kinetic data using eq 16 (see text for detail).

Resolved AdP Equilibrium Melting Curves Show Melting of α-Helix, π-Helix/Bulge, and 3_{10}-Helix Conformations. Recently, we showed that the "α-helix-like" UVRR spectra of AP, which is the natural abundance analogue of AdP contains contributions from π-bulges/helices and 3_{10}-helices.[171] Figure 5 shows the melting curves for AP (and thus AdP) and demonstrates that the pure α-helix, π-helix/bulge, and 3_{10}-helix conformations have different melting curves. The π-bulges/helices and 3_{10}-helices melt at lower temperatures than the pure α-helices and are fully melted by 30 °C. The decreased T_m values for the π-bulge and 3_{10}-helix conformations results from their less optimized intrapeptide hydrogen bonding compared to that of the α-helix. The more solvent exposed π-bulges[198] and 3_{10}-helices (type III turns)[199] populate due to the increased *peptide bond−water* hydrogen bond strengths at lower temperatures.[4,120,135,145]

The arrows in Figure 5 show the temperature intervals for the 5 → 30 and 20 → 40 °C T-jumps; Table 2 summarizes the equilibrium α-helical, 3_{10}-helical, and π-bulge/helical fractions of AdP at initial and final T-jump temperatures. Clearly, different conformations are melting to the PPII conformation at the different intial and final T-jump temperatures. These different conformations have different (un)folding rates and different relative contributions to the net AdP melting kinetics at the different temperatures (Figure 5).

Below, we show that the AdP π-bulge and 3_{10}-helix conformations have ∼12-fold faster unfolding rates than that of the pure α-helix conformation (Table 3). Thus, the lower temperature T-jumps predominantly sample the faster melting π-bulge and 3_{10}-helix conformations (Figure 5). In contrast, the higher temperature T-jump (Figure 5) samples a larger fraction of pure α-helix melting with slower (un)folding rates.

Pure AdP α-Helices at +30 and +40 °C Are Stabilized by ∼1.5 kcal/mol PB with Respect to π-Bulges and 3_{10}-Helices. Recently, we developed a method to estimate the Ψ Ramachandran angular population distributions of peptides and proteins from their UVRR $AmIII_3$ band profiles.[120,135,144,171,179] These Ψ angular population distributions can then be used to estimate the Gibbs free energy landscapes (GFELs) along the Ψ angle folding coordinate.[135,171]

Figure 6 shows the estimated GFELs for AdP at +30 and +40 °C, which are important in understanding the AdP kinetics. The +30 °C AdP GFEL (Figure 6A) was estimated exactly same way as for AP,[171] which is a natural abundance analogue of AdP. To estimate the +40 °C AdP GFEL (Figure 6B), we assumed that the Ψ angular distribution of the pure α-helix at +40 °C has the maximum value of Ψ = −42° and the same halfwidth, σ, of ∼5° as that at +30 °C.[171] This is a reasonable assumption, because we showed earlier that the ∼11 cm^{-1} half width at half-height (hwhh) of the +30 °C α-helical $AmIII_3$ UVRR band in water[171] is only slightly larger than the ∼7.5 cm^{-1} homogenous line width (HWHH) measured in peptide crystals.[120]

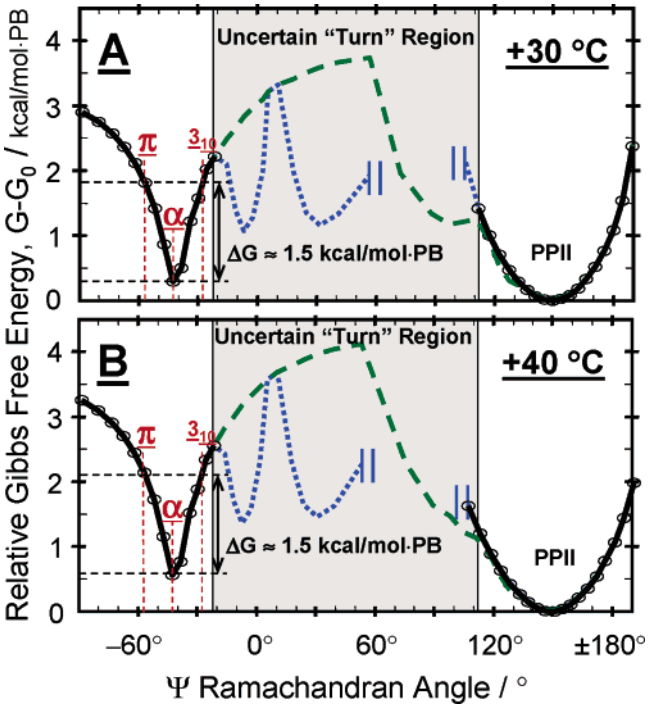

Figure 6. Relative Ψ angular Gibbs free energy landscapes (GFEL) for AdP at different temperatures. (A) +30 °C. (B) +40 °C. Black lines with circles represent well-determined portions of the GFEL in the α-helix and PPII regions of the Ramachandran plot. The dotted blue line in the uncertain "turn" regions of the Ramachandran plot assumes that the turns T1 and T2 exist at Ψ ≈ −10° and +30°, respectively.[171] The dashed green line assumes that turns T1 and T2 exist at Ψ ≈ +130° and +90°, respectively.[171]

The black lines in Figure 6 show the well determined portions of GFELs in the α-helical and PPII Ψ angular regions. This allows us to reliably determine the energy differences between pure α-helix, π-bulge, and 3_{10}-helix conformations of AdP, whose minima occur at Ψ angles of −42°, −58°, and −28°, respectively.[171] Specifically, we find that, at both +30 and +40 °C, the Gibbs free energies of π-bulges and 3_{10}-helices are approximately equal to each other. In contrast, the pure α-helix conformation is stabilized by ∼1.5 kcal/mol PB with respect to π-bulges and 3_{10}-helices (Figure 6), as expected.[56,93]

The dotted blue line in Figure 6 shows a very roughly estimated Ψ angle GFEL in the uncertain "turn" regions of the Ramachandran plot, by assuming that the detected minor turn conformations occur at Ψ ≈ −5° and +34°, respectively.[171] In this case, it is not possible to determine the portion of GFEL between Ψ values of ∼60° and 100°, nor to reliably determine the energy barrier between the α-helix and the PPII conformations (60° to 100°, Figure 6). However, we can estimate that the barriers at the other angles are <3.6 kcal/mol peptide bond (kcal/mol PB).

The dashed green line in Figure 6 shows another option for the GFEL in the "turn" region of the Ramachandran plot, which assumes that the turns T1 and T2 (or β-strand) exist at Ψ ≈ +133° and +94°, respectively.[171] Under this assumption, we estimate that the energy barriers between the α-helix and PPII conformations are between ∼3.5 and 4.2 kcal/mol PB (Figure 6).

Below, we use Figure 6 GFELs to relate the unfolding rate constants of pure α-helix, 3_{10}-helix, and π-bulge conformations.

Model for the Summed C_α−H and C_α−D Peptide Bonds AdP Kinetics. We expect that the relaxations of the π, 3_{10}, and α-helical conformations occur in parallel. This results in monoexponential relaxations for these conformations with relaxation times, which are determined by their activation free energy barriers, which separate each "α-helix-like" conformation from the PPII basin conformation. We expect identical attempt frequencies because the motions will involve similar Ψ torsional motions.

The relative contribution of each relaxation to the overall kinetics is determined by the differences in equilibrium fractions of each conformation between the final and initial T-jump temperatures (Table 2).

Thus, the time dependence of the fractional PPII conformation (summing both the C_α−H and C_α−D peptide bonds) subsequent to the T-jump is

$$f_{\mathrm{PPII}}^{T_i\rightarrow T_f}(t) \cong f_{\mathrm{PPII}}^{T_f}(\infty) - \Delta f_\pi \exp[-(k_U^\pi + k_F^\pi)t] - \Delta f_{310} \exp[-(k_U^{310} + k_F^{310})t] - \Delta f_\alpha \exp[-(k_U^\alpha + k_F^\alpha)t] \quad (9)$$

where $f_{\mathrm{PPII}}^{T_i\rightarrow T_f}(t)$ is the PPII fraction monitored at delay time t for the T-jump between the initial, T_i, and final temperatures, T_f; $f_{\mathrm{PPII}}^{T_f}(\infty)$ is the known equilibrium PPII fraction at T_f (Table 2); $\Delta f_{\pi,310,\alpha} = f_{\pi,310,\alpha}(T_i) - f_{\pi,310,\alpha}(T_f)$ are the known differences in the equilibrium fractions of the π, 3_{10}, and α-helical conformations at T_i and T_f (Table 2). $k_U^{\pi,310,\alpha}$ and $k_F^{\pi,310,\alpha}$ are the *unknown* unfolding and folding rate constants of the π-bulges, 3_{10}-helices, and α-helices, respectively, at T_f.

Inserting the corresponding α-helix, π-bulge, 3_{10}-helix, and PPII fractions from Table 2, we can describe the time dependence of the PPII fractions for the 5 → 30 °C and 20 → 40 °C T-jumps:

$$f_{\mathrm{PPII}}^{5\rightarrow 30^\circ\mathrm{C}}(t) = 0.77 - 0.2 \exp[-(k_U^\pi + k_F^\pi)t] - 0.09 \exp[-(k_U^{310} + k_F^{310})t] - 0.01 \exp[-(k_U^\alpha + k_F^\alpha)t] \quad (10A)$$

$$f_{\mathrm{PPII}}^{20\rightarrow 40^\circ\mathrm{C}}(t) = 0.84 - 0.11 \exp[-(k_U^\pi + k_F^\pi)t] - 0.06 \exp[-(k_U^{310} + k_F^{310})t] - 0.07 \exp[-(k_U^\alpha + k_F^\alpha)t] \quad (10B)$$

At the final T-jump temperatures of 30 and 40 °C, there are essentially no π-bulges and 3_{10}-helices left (Table 2 and Figure 5). Thus, $k_U^\pi \gg k_F^\pi$ and $k_U^{310} \gg k_F^{310}$, indicating that

$$f_{\mathrm{PPII}}^{5\rightarrow 30^\circ\mathrm{C}}(t) \cong 0.77 - 0.2 \exp[-k_U^\pi t] - 0.09 \exp[-k_U^{310} t] - 0.01 \exp[-(k_U^\alpha + k_F^\alpha)t] \quad (11A)$$

$$f_{\mathrm{PPII}}^{20\rightarrow 40^\circ\mathrm{C}}(t) \cong 0.84 - 0.11 \exp[-k_U^\pi t] - 0.06 \exp[-k_U^{310} t] - 0.07 \exp[-(k_U^\alpha + k_F^\alpha)t] \quad (11B)$$

As discussed above (Figure 6), the Gibbs free energy activation barriers for unfolding of the π-bulge and 3_{10}-helix conformations are essentially identical. Thus, their unfolding rate constants will be equal and

$$f_{\mathrm{PPII}}^{5\rightarrow 30^\circ\mathrm{C}}(t) \cong 0.77 - 0.29 \exp[-k_U^\pi t] - 0.01 \exp[-(k_U^\alpha + k_F^\alpha)t] \quad (12A)$$

$$f_{\mathrm{PPII}}^{20\rightarrow 40^\circ\mathrm{C}}(t) \cong 0.84 - 0.17 \exp[-k_U^\pi t] - 0.07 \exp[-(k_U^\alpha + k_F^\alpha)t] \quad (12B)$$

Also as shown above (Figure 6), the AdP pure α-helix conformation is stabilized by ∼1.5 kcal/mol PB with respect to both π-bulge and 3_{10}-helix conformations. Thus, we can

estimate the ratio between the α-helix and π-bulge (3_{10}-helix) unfolding rate constants as

$$k_U^{\pi} \approx k_U^{310} \cong k_U^{\alpha} \exp\left(+\frac{1.5\ \text{kcal/mol}}{RT}\right) \quad (13)$$

Thus, we estimate that at 30 °C $k_U^{\pi} \approx k_U^{310} \cong 12.1 k_U^{\alpha}$, whereas at 40 °C $k_U^{\pi} \approx k_U^{310} \cong 11.1 k_U^{\alpha}$.

Because only pure α-helix remains at the T_f values of 30 and 40 °C. Thus,

$$k_F^{\alpha} = K_{EQ}^{-1} k_U^{\alpha} = \frac{f_{\alpha}(T_f)}{f_{PPII}(T_f)} k_U^{\alpha} \quad (14)$$

where $K_{EQ} = f_{PPII}(T_f)/f_{\alpha}(T_f) = k_U^{\alpha}/k_F^{\alpha}$ is the known equilibrium constant for the pure α-helix ↔ PPII melting (Tables 1 and 3); $f_{\alpha,PPII}(T_f)$ are the known equilibrium pure α-helix and PPII fractions at T_f (Table 2).

Thus, we estimate that the "apparent two-state relaxation constant" at +30 °C to be

$$k_U^{\alpha} + k_F^{\alpha} \cong 1.3 k_U^{\alpha} \cong 0.11 k_U^{\pi}$$

and at +40 °C to be

$$k_U^{\alpha} + k_F^{\alpha} \cong 1.2 k_U^{\alpha} \cong 0.11 k_U^{\pi}$$

Thus, we can further simplify eqs 12A and 12B:

$$f_{PPII}^{5\rightarrow 30^{\circ}C}(t) \cong 0.77 - 0.29 \exp[-k_U^{\pi} t] - 0.01 \exp[-(0.11 k_U^{\pi}) t] \quad (15A)$$

$$f_{PPII}^{20\rightarrow 40^{\circ}C}(t) \cong 0.84 - 0.17 \exp[-k_U^{\pi} t] - 0.07 \exp[-(0.11 k_U^{\pi}) t] \quad (15B)$$

The eq 15A fit to the summed C_α−H and C_α−D peptide bond kinetics (Figure 4A dotted line) is slightly improved compared with the original monoexponential fit (Figure 4A solid line); the eq 15B fit (Figure 4B dotted line) is significantly improved compared with the monoexponential fit (Figure 4B solid line).

Specifically, the pure α-helix relaxation time (τ_R) at +30 °C is 1017 ± 148 ns; the relaxation times for the π-bulge and 3_{10}-helix conformations at +30 °C are much faster, 109 ± 16 ns (Table 3). At 40 °C, the relaxation times decrease; the pure α-helix relaxation time at +40 °C is 568 ± 165 ns, and the π-bulge and 3_{10}-helix conformation relaxation times decrease to 61 ± 18 ns. These results are striking, because they indicate that the pure α-helix melting is much slower than the 100−200 ns times, which are typically reported for ~20 residue-long Ala-rich peptides.[4−6,10,13,17,18,22,25,32−35] This discrepancy derives from the previous inability to discriminate between the different α-helix-like conformations (Figure 5 and Table 3).

In addition, we estimated from our kinetic data that a 5.4−19.8 kcal/mol PB *unfolding* and 0−11.3 kcal/mol PB *folding* Gibbs free energy activation barriers exist between the α-helix and PPII conformations (Table 3). The higher kinetic activation barrier found for unfolding (Table 3) than that estimated from the equilibrium GFELs (Figure 6) may indicate the existence of the additional intermediate states involved in the α-helix unfolding reaction of AdP. These additional states would slow down the α-helix unfolding rates at low temperatures, making the serial calculated unfolding free energy activation barrier higher than any of the individual barriers.

Further, our results here explain the complicated nonexponential and/or multiexponential behavior of melting kinetics of Ala-rich peptides previously observed.[22,34] Specifically, the heterogeneity of the low temperature α-helical ensembles (Figure 5) explains the observed complicated kinetic behavior for low initial T-jump temperatures.[22,34] In contrast, the homogeneity of the above room temperature α-helical ensembles (Figure 5) explains the essentially monoexponential melting behavior of these peptides for higher initial temperature T-jumps.[22,34]

Model for Individual C_α−H Center and C_α−D End Peptide Bonds Melting Kinetics. Table 3 summarizes our pure α-helix, π-bulge, and 3_{10}-helix folding and unfolding rate constants that we determined by fitting the overall (C_α−D plus C_α−H peptide bond) kinetic data to eq 15. If we assume that the (un)folding rates of the π, 3_{10}, and α-helical conformations are independent of location along the AdP chain, we can estimate the relative contributions of both the slow α-helix melting and the fast 3_{10}-helix and π-bulge melting to the observed individual relaxation kinetics of C_α−D *end* and C_α−H *center* peptide bonds using the following equation:

$$f_{PPII}^{T_i\rightarrow T_f}(t) \cong f_{PPII}^{T_f}(\infty) - \Delta a_{\pi+310}^{Ind} \exp[-t/\tau_{\pi+310}] - \Delta f_{\alpha}^{Ind} \exp[-t/\tau_{\alpha}] \quad (16)$$

where $f_{PPII}^{T_i\rightarrow T_f}(t)$ is the time-dependent PPII concentration for the C_α−D or the C_α−H peptide bonds; $f_{PPII}^{T_f}(\infty)$ is the known equilibrium C_α−D or C_α−H peptide bond PPII fraction at T_f (Tables 1 and 3); $\Delta f_{\pi+310}^{Ind} A_{\pi+310}$ is the *unknown* weighted contribution of π-bulges and 3_{10}-helices melting to the observed individual C_α−D (or C_α−H) peptide bond kinetics; Δf_{α}^{Ind} is the *unknown* weighted contribution of pure α-helix melting to the observed individual C_α−D (or C_α−H) peptide bond kinetics; and τ_α and $\tau_{\pi+310}$ are the known relaxation times for the pure α-helix, π-bulge, and 3_{10}-helix conformations (Table 3).

Thus, we find the relative contributions of the slow α-helix melting (Δf_{α}^{Ind}) and fast 3_{10}-helix and π-bulge melting ($\Delta f_{\pi+310}^{Ind}$) to the observed individual relaxation kinetics of C_α−D *end* and C_α−H *center* peptide bonds (after the 5 → 30 and 20 → 40 °C T-jumps) by fitting the experimental data (Figure 4C−F) to eq 16 above. The calculated fractions are summarized in Table 3.

Dynamics of End C_α−D Peptide Bond Unfolding. Figure 4C, D shows the time dependence of the calculated PPII concentration of the C_α−D ends peptide bonds as a result of the T-jumps from 5 to 30 and 20 to 40 °C, respectively. If the time-dependent changes in the C_α−D peptide bond PPII concentration were modeled assuming monoexponential decays, we find that the C_α−D end peptide bonds show a relaxation time (k_{R-Ends}^{-1}) of 97 ± 15 ns (Figure 6C) for the 5 to 30 °C T-jump, whereas for the 20 to 40 °C T-jump we obtain a relaxation time of 131 ± 46 ns (Figure 4D).

The fast monoexponential relaxation time of 97 ± 15 ns found for the 5 to 30 °C T-jump (Figure 4C and Table 3) indicates that the melting kinetics of C_α−D end peptide bonds is contributed mainly by the melting of π-bulges and 3_{10}-helices (109 ± 16 ns at +30 °C). Using eq 16, we estimate that the C_α−D end kinetics is essentially completely due to melting of π-bulges and 3_{10}-helices, without contributions from pure α-helix melting for the 5 to 30 °C T-jump (Figure 4C and Table 3).

In contrast, the relaxation time of 131 ± 46 ns found for the 20 to 40 °C T-jump (Figure 4D and Table 3) indicates that, in addition to fast π-bulge and 3_{10}-helix melting (61 ± 18 ns at

+40 °C), there is also a contribution of slow α-helix melting (568 ± 165 ns at +40 °C). Using eq 16, we roughly estimate that in this case the C_α−D end peptide bonds kinetics is still dominated by the melting of π-bulges and 3_{10}-helices (∼65%), but there is also a ∼35% contribution from the pure α-helix melting of (Figure 4D and Table 3).

Summarizing, we observe that the melting kinetics of C_α−D end peptide bonds is dominated by the faster melting of π-bulges and 3_{10}-helices over the slower melting of pure α-helices for both 5 → 30 and 20 → 40 °C T-jumps. These results are consistent with a number of recent studies, which propose that the α-helical ends are frayed.[7,25,28,29,31,32,37,43,75,80] They are also consistent with the recent NMR and ESR results of Millhauser and co-workers[159,164] as well as with that of Sorin and Pande's MD simulation studies,[72] which report that 3_{10}-helices tend to occur at the ends of α-helical segments in Ala rich peptides.

Dynamics of Center C_α−H Peptide Bond Unfolding. Figure 4E, F shows the time-dependent changes in the PPII concentration of the central AdP C_α−H peptide bonds due to the T-jumps from 5 to 30 and from 20 to 40 °C. The unfolding kinetics of C_α−H peptide bonds shown in Figure 4E, F depends upon the T-jump initial and final temperatures. We find that for the 5 to 30 °C T-jump the C_α−H peptide bonds show a 189 ± 31 ns monoexponential unfolding relaxation time (Figure 4E), and for the 20 to 40 °C T-jump, we obtained 56 ± 6 ns as a relaxation time (Figure 4F).

The 189 ± 31 ns monoexponential relaxation time calculated for the 5 to 30 °C T-jump (Figure 4C and Table 3) indicates that the slow α-helix melting (1017 ± 148 ns at 30 °C) contributes to the observed kinetics. However, the observed kinetics is dominated by the fast π-bulge and 3_{10}-helix melting (109 ± 16 ns at 30 °C). Using eq 16 (Figure 4D dotted line), we roughly estimate a ∼73% contribution from the π-bulges and 3_{10}-helices to the C_α−H center peptide bonds kinetics and a ∼27% contribution from pure α-helix melting (Figure 4D and Table 3).

In contrast, the 56 ± 6 ns monoexponential relaxation time found for the 20 to 40 °C T-jump (Figure 4D, Table 3) surprisingly indicates that the C_α−H center peptide bond kinetics are dominated by π-bulge and 3_{10}-helix melting (61 ± 18 ns at 40 °C), with little contribution of slow α-helix melting (568 ± 165 ns at 40 °C). This is a surprising result, because at 20 °C "α-helix-like" segments[6] are assumed to preferentially occur in the middle of the peptide, and thus, α-helix melting should dominate the observed C_α−H center peptide bond kinetics. This suggests that the α-helix stability/propensity in AdP is position-dependent (see below). Specifically, we suggest below that the AdP N-terminus has the higher α-helical propensity than does the AdP middle and C-terminal regions.

Dynamics of Center C_α−H Versus End C_α−D Peptide Bond Unfolding. Figure 4C, E shows that, for the 5 to 30 °C T-jump, the AdP center unfolds slower (189 ± 31 ns) than do the ends (97 ± 15 ns). We also estimated that at 30 °C the relaxation time of pure α-helices is 1017 ± 148 ns, whereas that of π-bulges and 3_{10}-helices is 109 ± 16 ns (Table 3). If the relaxation rates of these "α-helix-like" species are independent of location in the AdP chain, we can conclude that the melting of π-bulges and 3_{10}-helices dominate both the AdP C_α−D ends (∼100%) and C_α−H center (∼73%) melting kinetics (Table 3). However, pure α-helix melting also has a small contribution (∼27%) to the C_α−H center melting kinetics for the 5 to 30 °C T-jump (Table 3). These kinetic results are consistent with the Figure 5 equilibrium melting curves obtained for pure α-helix, π-bulge, and 3_{10}-helix conformations,[171] as well as with the earlier studies of us[7] and others,[12,23,25,28,29,31,37,43,75,80] which indicate that the ends of AdP-like peptides are frayed.

In contrast, for the 20 to 40 °C T-jump, the center of AdP unfolds faster (56 ± 6 ns, Figure 4F) than do the ends (131 ± 46 ns, Figure 4D). The faster center melting for the 20 to 40 °C T-jump, especially given the higher T_m of the center peptide bonds,[7] appears initially surprising. We suggest that the faster melting of π-bulges and 3_{10}-helices still dominate both the C_α−H center (∼93%) and C_α−D ends (∼65%) melting kinetics. However, we surprisingly find that the pure α-helix melting contributes ∼35% to the C_α−D ends melting kinetics and contributes very little to the C_α−H center kinetics (Table 3). These results can only be understood if one of the AdP termini has a significantly higher pure α-helix propensity than the AdP center and the other terminus.

We propose that the AdP N-terminus has a higher α-helix propensity than the middle and C-terminus. Such a preference would derive from the AdP primary sequence. Specifically, the N-terminus of AdP contains a sequence of eight Ala, which stabilize the α-helix conformation.[52] In contrast, three hydrophilic Arg are distributed within the AdP center and C-terminus. These three Arg partially destabilize the α-helices and favor formation of the water-mediated α-helical defects such as π-bulges[198] and 3_{10}-helices.[199]

At first sight, our results contradict Vila et al.'s theoretical study,[200] which suggests that polar long side chains (such as Arg) stabilize the α-helix by protecting the helical amides from water hydrogen bonding. However, Vila et al.'s studies ignored side chain charge−charge interactions, which are absent in their peptide but are present in AdP. A more realistic approximation of the AdP case is provided by the NMR and CD studies of Kallenbach's group,[52] where the guest charged residue (Lys or ornithine) is inserted inside the Ala sequence flanked by other charged residues. In accordance with our findings, Kallenbach's studies also clearly show that charged residues destabilize the α-helix conformation.

The higher α-helix stability at the AdP N-terminus also agrees well with the MD simulation studies of Sorin and Pande,[72] which suggested that the N-terminus of 21-residue α-helical Fs-peptide (which is a natural abundance analogue of AdP) has a higher α-helical content than occurs in the middle and at the C-terminus. These MD studies also suggest that the arginines destabilize α-helices in Fs (and thus in AdP). We suggest that these hydrophilic Arg are likely not only to partially destabilize α-helices but also induce the formation of water-mediated α-helical defects such as π-bulges[198] and 3_{10}-helices (type III turns)[199] at low temperatures, at which the peptide bond−water hydrogen-bonding strength increases.[120,135,145]

Whatever the case, our calculated ∼4.4 and ∼1.3 μs (+30 °C) and ∼3.6 and ∼0.7 μs (+40 °C) pure α-helix folding and unfolding times (Table 3), respectively, are much slower than the (un)folding times previously reported for similar peptides. It is now obvious that the ∼100−200 ns relaxation times typically reported for Ala-rich peptides[4−6,10,13,17,18,22,25,32−35,120] signal the dominating contribution of π-bulge and/or 3_{10}-helix melting to the observed overall relaxation kinetics. In addition, it is also clear that at least some of the observed deviations from the monoexponential behavior[22,33,34] for Ala-rich peptide melting result from the temperature dependence of the relative contributions of pure α-helices, π-bulges, and 3_{10}-helices melting to the overall relaxation kinetics. We believe our results here are the first experimental ones to resolve the kinetic behavior of the different α-helix-like conformations.

The ~10-fold slower pure α-helix melting and formation rates found for AdP deserve the attention of theoreticians and experimentalists. Specifically, this decreased pure α-helix melting rate will significantly impact the competition between the parallel folding of different structural motifs.

Conclusions

We examined the relaxation kinetics of 21-amino acid residues (mainly the Ala peptide AdP, which contains three Arg to give solubility). This peptide is ≥55% α-helix-like at 0 °C and melts to a PPII conformation at higher temperature. Previous isotopic substitution studies demonstrated a significantly higher $T_m = 32$ °C for the 6 center residues compared to a $T_m = 5$ °C for the end residues.[7] We used T-jump measurements to examine the melting kinetics. We find that the middle AdP peptide bonds show a relaxation time ~2-fold slower than the end residues for the 5 to 30 °C T-jump. In contrast, for a 20 to 40 °C T-jump, the middle AdP peptide bonds appear to show faster kinetics than the end AdP peptide bonds.

We explain the observed kinetics in terms of different relative contributions of different α-helix-like motifs such as pure α-helices, π-bulges, and 3_{10}-helices to the observed melting kinetics. We estimated that the melting rate constant of pure α-helices is ~12-fold slower than those of π-bulges and 3_{10}-helices (Table 3). This strikingly suggests that the pure α-helix (un)folding occurs at a microsecond time scale at room temperature.

For the 5 to 30 °C T-jump, the faster melting of π-bulges and 3_{10}-helices dominate both the AdP ends and center kinetics, with also a minor contribution of slower pure α-helix melting to the AdP center kinetics. In contrast, for the 20 to 40 °C T-jump, the faster melting of π-bulges and 3_{10}-helices dominates both the AdP ends and center kinetics, whereas there is also a minor contribution of slower pure α-helix melting to the AdP ends kinetics. These surprising results can be explained in terms of a higher pure α-helical propensity at the AdP N-terminus compared with the middle and C-terminus.

The higher stability of the pure α-helix at the AdP N-terminus can be understood in terms of AdP primary sequence. Specifically, three hydrophilic Arg located in the AdP middle and at the AdP C-terminus destabilize the pure α-helices and induce formation of water-mediated α-helical defects (such as π-bulges and 3_{10}-helices), which melt faster.

In addition, we developed a kinetic model to calculate the (un)folding rate constants for pure α-helices, π-bulges, and 3_{10}-helices. We successfully explain the apparent anti-Arrhenius behavior observed earlier by Lednev et al.[4] as resulting from the parallel melting of these different conformations. Further, our model also explains the complicated nonexponential behavior observed earlier by Huang et al.[34] and Bredenbeck et al.[22] for similar peptides.

Summarizing, we believe that our results here are the first experimental ones to quantitatively show that the folding mechanism of end residues of Ala-rich peptides significantly differs from that of middle residues in terms of different relative contributions of different "α-helix-like" species to the melting kinetics. In addition, we for the first time measured the kinetic (un)folding rate constants for pure α-helices, 3_{10}-helices, and π-bulges in Ala-rich peptides of ~20 residues long. Thus, our results not only directly demonstrate that α-helix melting and formation in peptides are not a simple two-state processes but also provide an important quantitative basis for testing theoretical studies in the field of peptide and protein folding.

Acknowledgment. We gratefully acknowledge Ahmed Zeeshan, Bhavya Sharma, Konstantin Pimenov, Dr. Jon Scaffidi, and Dr. Natalyia Myshakina for useful discussions. We thank Dr. Leon J. Gleser, Dr. Sunil Saxena, and Dr. Carlos Gomes for their assistance in the statistical evaluation. We also thank Mr. Anton Karnoup who performed the MALDI MS analysis to verify the AdP sequence. This work was supported by NIH grant GM8RO1EB002053-24.

References and Notes

(1) Creighton, T. E. *Protein Structure,* 2nd ed.; IRL: Oxford, U.K., 1997.
(2) Zimm, B. H.; Bragg, J. K. *J. Chem. Phys.* **1959**, *31*, 526.
(3) Poland, D.; Scheraga, H. A. *J. Phys. Chem.* **1966**, *45*, 2071.
(4) Lednev, I. K.; Karnoup, A. S.; Sparrow, M. C.; Asher, S. A. *J. Am. Chem. Soc.* **1999**, *121*, 8074.
(5) Lednev, I. K.; Karnoup, A. S.; Sparrow, M. C.; Asher, S. A. *J. Am. Chem. Soc.* **1999**, *121*, 4076.
(6) Lednev, I. K.; Karnoup, A. S.; Sparrow, M. C.; Asher, S. A. *J. Am. Chem. Soc.* **2001**, *123*, 2388.
(7) Ianoul, A.; Mikhonin, A.; Lednev, I. K.; Asher, S. A. *J. Phys. Chem. A* **2002**, *106*, 3621.
(8) Lockhart, D. J.; Kim, P. S. *Science* **1992**, *257*, 947.
(9) Lockhart, D. J.; Kim, P. S. *Science* **1993**, *260*, 198.
(10) Werner, J. H.; Dyer, R. B.; Fesinmeyer, R. M.; Andersen, N. H. *J. Phys. Chem. B* **2002**, *106*, 487.
(11) Gruebele, M. *Annu. Rev. Phys. Chem.* **1999**, *50*, 485.
(12) Fesinmeyer, R. M.; Peterson, E. S.; Dyer, R. B.; Andersen, N. H. *Protein Sci.* **2005**, *14*, 2324.
(13) Williams, S.; Causgrove, T. P.; Gilmanshin, R.; Fang, K. S.; Callender, R. H.; Woodruff, W. H.; Dyer, R. B. *Biochemistry* **1996**, *35*, 691.
(14) Dyer, R. B.; Gai, F.; Woodruff, W. H.; Gilmanshin, R.; Callender, R. H. *Acc. Chem. Res.* **1998**, *31*, 709.
(15) Callender, R.; Dyer, R. B.; Gilmanshin, R.; Woodruff, W. H. *Annu. Rev. Phys. Chem.* **1998**, *49*, 173.
(16) Causgrove, T. P.; Dyer, R. B. *Chem. Phys.* **2006**, *323*, 2.
(17) Thompson, P. A.; Eaton, W. A.; Hofrichter, J. *Biochemistry* **1997**, *36*, 9200.
(18) Thompson, P. A.; Munoz, V.; Jas, G. S.; Henry, E. R.; Eaton, W. A.; Hofrichter, J. *J. Phys. Chem. B* **2000**, *104*, 378.
(19) Kubelka, J.; Hofrichter, J.; Eaton, W. A. *Curr. Opin. Struct. Biol.* **2004**, *14*, 76.
(20) Lapidus, L. J.; Eaton, W. A.; Hofrichter, J. *Proc. Natl. Acad. Sci. U.S.A.* **2000**, *97*, 7220.
(21) Lapidus, L. J.; Eaton, W. A.; Hofrichter, J. *J. Mol. Biol.* **2002**, *319*, 19.
(22) Bredenbeck, J.; Helbing, J.; Kumita, J. R.; Woolley, G. A.; Hamm, P. *Proc. Natl. Acad. Sci. U.S.A.* **2005**, *102*, 2379.
(23) Decatur, S. M.; Antonic, J. *J. Am. Chem. Soc.* **1999**, *121*, 11914.
(24) Decatur, S. M. *Biopolymers* **2000**, *54*, 180.
(25) Ramajo, A. P.; Petty, S. A.; Starzyk, A.; Decatur, S. M.; Volk, M. *J. Am. Chem. Soc.* **2005**, *127*, 13784.
(26) Pozo, Ramajo, A.; Petty, S. A.; Volk, M. *Chem. Phys.* **2006**, *323*, 11.
(27) Gooding, E. A.; Ramajo, A. P.; Wang, J.; Palmer, C.; Fouts, E.; Volk, M. *Chem. Commun.* **2005**, 5985.
(28) Silva, R. A.; Kubelka, J.; Bour, P.; Decatur, S. M.; Keiderling, T. A. *Proc. Natl. Acad. Sci. U.S.A.* **2000**, *97*, 8318.
(29) Yoder, G.; Pancoska, P.; Keiderling, T. A. *Biochemistry* **1997**, *36*, 15123.
(30) (a) Keiderling, T. A.; Silva, R. A.; Yoder, G.; Dukor, R. K. *Bioorg. Med. Chem.* **1999**, *7*, 133. (b) Dukor, R. K.; Keiderling, T. A. *Biopolymers* **1991**, *31*, 1747.
(31) Decatur, S. M. *Acc. Chem. Res.* **2006**, *39*, 169.
(32) Huang, C.-Y.; Getahun, Z.; Wang, T.; DeGrado, W. F.; Gai, F. *J. Am. Chem. Soc.* **2001**, *123*, 12111.
(33) Huang, C.-Y.; Getahun, Z.; Zhu, Y.; Klemke, J. W.; DeGrado, W. F.; Gai, F. *Proc. Natl. Acad. Sci. U.S.A.* **2002**, *99*, 2788.
(34) Huang, C.-Y.; Klemke, J. W.; Getahun, Z.; DeGrado, W. F.; Gai, F. *J. Am. Chem. Soc.* **2001**, *123*, 9235.
(35) Wang, T.; Zhu, Y.; Getahun, Z.; Du, D.; Huang, C.-Y.; DeGrado, W. F.; Gai, F. *J. Phys. Chem. B* **2004**, *108*, 15301.
(36) Wang, T.; Du, D.; Gai, F. *Chem. Phys. Lett.* **2003**, *370*, 842.
(37) Rohl, C. A.; Baldwin, R. L. *Biochemistry* **1994**, *33*, 7760.
(38) Chakrabartty, A.; Kortemme, T.; Baldwin, R. L. *Protein Sci.* **1994**, *3*, 843.
(39) Scholtz, J. M.; Marqusee, S.; Baldwin, R. L.; York, E. J.; Stewart, J. M.; Santoro, M.; Bolen, D. W. *Proc. Natl. Acad. Sci. U.S.A.* **1991**, *88*, 2854.

(40) Marqusee, S.; Baldwin, R. L. *Proc. Natl. Acad. Sci. U.S.A.* **1987**, *84*, 8898.
(41) Marqusee, S.; Robbins, V. H.; Baldwin, R. L. *Proc. Natl. Acad. Sci. U.S.A.* **1989**, *86*, 5286.
(42) Padmanabhan, S.; Marqusee, S.; Ridgeway, T.; Laue, T. M.; Baldwin, R. L. *Nature* **1990**, *344*, 268.
(43) Venyaminov, S. Y.; Hedstrom, J. F.; Prendergast, F. G. *Proteins* **2001**, *45*, 81.
(44) Cochran, D. A. E.; Doig, A. J. *Protein Sci.* **2001**, *10*, 1305.
(45) Cochran, D. A. E.; Penel, S.; Doig, A. J. *Protein Sci.* **2001**, *10*, 463.
(46) Miller, J. S.; Kennedy, R. J.; Kemp, D. S. *Biochemistry* **2001**, *40*, 305.
(47) Kennedy, R. J.; Walker, S. M.; Kemp, D. S. *J. Am. Chem. Soc.* **2005**, *127*, 16961.
(48) Heitmann, B.; Job, G. E.; Kennedy, R. J.; Walker, S. M.; Kemp, D. S. *J. Am. Chem. Soc.* **2005**, *127*, 1690.
(49) Goch, G.; Maciejczyk, M.; Oleszczuk, M.; Stachowiak, D.; Malicka, J.; Bierzynski, A. *Biochemistry* **2003**, *42*, 6840.
(50) Gans, P. J.; Lyu, P. C.; Manning, M. C.; Woody, R. W.; Kallenbach, N. R. *Biopolymers* **1991**, *31*, 1605.
(51) Kallenbach, N. R.; Lyu, P.; Zhou, H. *Circ. Dichroism Conform. Anal. Biomol.* **1996**, 201.
(52) Spek, E. J.; Olson, C. A.; Shi, Z.; Kallenbach, N. R. *J. Am. Chem. Soc.* **1999**, *121*, 5571.
(53) Doruker, P.; Bahar, I. *Biophys. J.* **1997**, *72*, 2445.
(54) Scholtz, J. M.; Qian, H.; York, E. J.; Stewart, J. M.; Baldwin, R. L. *Biopolymers* **1991**, *31*, 1463.
(55) Scholtz, J. M.; Baldwin, R. L. *Annu. Rev. Biophys. Biomol. Struct.* **1992**, *21*, 95.
(56) Young, W. S.; Brooks, C. L. III. *J. Mol. Biol.* **1996**, *259*, 560.
(57) Shirley, W. A.; Brooks, C. L. III. *Proteins* **1997**, *28*, 59.
(58) Tobias, D. J.; Brooks, C. L. III. *Biochemistry* **1991**, *30*, 6059.
(59) Brooks, C. L. III. *J. Phys. Chem.* **1996**, *100*, 2546.
(60) Ohkubo, Y. Z.; Brooks, C. L. III. *Proc. Natl. Acad. Sci. U.S.A.* **2003**, *100*, 13916.
(61) Garcia, A. E.; Sanbonmatsu, K. Y. *Proc. Natl. Acad. Sci. U.S.A.* **2002**, *99*, 2782.
(62) Gnanakaran, S.; Garcia, A. E. *Proteins* **2005**, *59*, 773.
(63) Hummer, G.; Garcia, A. E.; Garde, S. *Phys. Rev. Lett.* **2000**, *85*, 2637.
(64) Hummer, G.; Garcia, A. E.; Garde, S. *Proteins* **2001**, *42*, 77.
(65) Nymeyer, H.; Garcia, A. E. *Proc. Natl. Acad. Sci. U.S.A.* **2003**, *100*, 13934.
(66) Paschek, D.; Gnanakaran, S.; Garcia, A. E. *Proc. Natl. Acad. Sci. U.S.A.* **2005**, *102*, 6765.
(67) Daggett, V.; Levitt, M. *J. Mol. Biol.* **1992**, *223*, 1121.
(68) Fitzkee, N. C.; Rose, G. D. *Protein Sci.* **2004**, *13*, 633.
(69) Doshi, U.; Munoz, V. *Chem. Phys.* **2004**, *307*, 129.
(70) Doshi, U. R.; Munoz, V. *J. Phys. Chem. B* **2004**, *108*, 8497.
(71) Munoz, V.; Serrano, L. *J. Mol. Biol.* **1995**, *245*, 297.
(72) Sorin, E. J.; Pande, V. S. *Biophys. J.* **2005**, *88*, 2472.
(73) Sorin, E. J.; Pande, V. S. *J. Comput. Chem.* **2005**, *26*, 682.
(74) Sorin, E. J.; Rhee, Y. M.; Shirts, M. R.; Pande, V. S. *J. Mol. Biol.* **2006**, *356*, 248.
(75) Zagrovic, B.; Jayachandran, G.; Millett, I. S.; Doniach, S.; Pande, V. S. *J. Mol. Biol.* **2005**, *353*, 232.
(76) Bertsch, R. A. *The early events of protein folding: simulations of polyalanine folding into an alpha-helix*; California Institute of Technology: Pasadena, CA, 1998.
(77) Bertsch, R. A.; Vaidehi, N.; Chan, S. I.; Goddard, W. A. III. *Proteins* **1998**, *33*, 343.
(78) Ferrara, P.; Apostolakis, J.; Caflisch, A. *J. Phys. Chem. B* **2000**, *104*, 5000.
(79) Irbaeck, A.; Mohanty, S. *Biophys. J.* **2005**, *88*, 1560.
(80) Doig, A. J. *Biophys. Chem.* **2002**, *281,* 101−102.
(81) Doig, A. J.; Errington, N.; Iqbalsyah, T. M. *Protein Folding Handbook* **2005**, *1*, 247.
(82) Kim, J. G.; Fukunishi, Y.; Nakamura, H. *Chem. Phys. Lett.* **2004**, *392*, 34.
(83) Levy, Y.; Jortner, J.; Becker, O. M. *Proc. Natl. Acad. Sci. U.S.A.* **2001**, *98*, 2188.
(84) Nguyen, H. D.; Marchut, A. J.; Hall, C. K. *Protein Sci.* **2004**, *13*, 2909.
(85) Peng, Y.; Hansmann, U. H. E.; Alves, N. A. *J. Chem. Phys.* **2003**, *118*, 2374.
(86) Takano, M.; Yamato, T.; Higo, J.; Suyama, A.; Nagayama, K. *J. Am. Chem. Soc.* **1999**, *121*, 605.
(87) Takano, M.; Nagayama, K.; Suyama, A. *J. Chem. Phys.* **2002**, *116*, 2219.
(88) Takano, M.; Nakamura, H. K.; Nagayama, K.; Suyama, A. *J. Chem. Phys.* **2003**, *118*, 10312.
(89) Mortenson, P. N.; Evans, D. A.; Wales, D. J. *J. Chem. Phys.* **2002**, *117*, 1363.
(90) Ulmschneider, J. P.; Jorgensen, W. L. *J. Chem. Phys.* **2003**, *118*, 4261.
(91) Ulmschneider, J. P.; Jorgensen, W. L. *J. Am. Chem. Soc.* **2004**, *126*, 1849.
(92) Tirado-Rives, J.; Jorgensen, W. L. *Biochemistry* **1991**, *30*, 3864.
(93) Tirado-Rives, J.; Maxwell, D. S.; Jorgensen, W. L. *J. Am. Chem. Soc.* **1993**, *115*, 11590.
(94) Mitsutake, A.; Okamoto, Y. *J. Chem. Phys.* **2000**, *112*, 10638.
(95) Samuelson, S.; Martyna, G. J. *J. Phys. Chem. B* **1999**, *103*, 1752.
(96) Hansmann, U. H. E.; Okamoto, Y. *J. Chem. Phys.* **1999**, *110*, 1267.
(97) Wu, X.; Wang, S. *J. Phys. Chem. B* **2001**, *105*, 2227.
(98) Wang, Y.; Kuczera, K. *J. Phys. Chem. B* **1997**, *101*, 5205.
(99) Van, Giessen, A. E.; Straub, J. E. *J. Chem. Theory Comput.* **2006**, *2*, 674.
(100) Chakrabartty, A.; Baldwin, R. L. *Adv. Protein Chem.* **1995**, *46*, 141.
(101) Chakrabartty, A.; Schellman, J. A.; Baldwin, R. L. *Nature* **1991**, *351*, 586.
(102) Arashiro, E.; Drugowich de Felicio, J. R.; Hansmann, U. H. E. *Phys. Rev. E* **2006**, *73*, 040902/1.
(103) Soto, P.; Mark, A. E. *J. Phys. Chem. B* **2002**, *106*, 12830.
(104) Peng, Y.; Hansmann, U. H. E. *Biophys. J.* **2002**, *82*, 3269.
(105) Smith, A. V.; Hall, C. K. *Proteins* **2001**, *44*, 344.
(106) Alves, N. A.; Hansmann, U. H. E. *Physica A* **2001**, *292*, 509.
(107) Pellegrini, M.; Gronbech-Jensen, N.; Doniach, S. *Physica A* **1997**, *239*, 244.
(108) Klein, C. T.; Mayer, B.; Koehler, G.; Wolschann, P. *THEOCHEM* **1996**, *370*, 33.
(109) Hoffmann, D.; Knapp, E.-W. *Eur. Biophys. J.* **1996**, *24*, 387.
(110) Scheraga, H. A.; Vila, J. A.; Ripoll, D. R. *Biophys. Chem.* **2002**, *255,* 101−102.
(111) Zhang, W.; Lei, H.; Chowdhury, S.; Duan, Y. *J. Phys. Chem. B* **2004**, *108*, 7479.
(112) Rathore, N.; Yan, Q.; de Pablo, J. J. *J. Chem. Phys.* **2004**, *120*, 5781.
(113) Agostini, F. P.; Soares-Pinto, D. D. O.; Moret, M. A.; Osthoff, C.; Pascutti, P. G. *J. Comput. Chem.* **2006**, *27*, 1142.
(114) Baumketner, A.; Shea, J. E. *Phys. Rev. E* **2003**, *68*, 051901/1.
(115) Baumketner, A.; Shea, J. E. *Condens. Matter Phys.* **2004**, *38*, 421.
(116) Ho, B. K.; Dill, K. A. *PLoS Comput. Biol.* **2006**, *2*, 228.
(117) Mezei, M.; Fleming, P. J.; Srinivasan, R.; Rose, G. D. *Proteins* **2004**, *55*, 502.
(118) Kentsis, A.; Mezei, M.; Gindin, T.; Osman, R. *Proteins* **2004**, *55*, 493.
(119) Blanch, E. W.; Morozova-Roche, L. A.; Cochran, D. A. E.; Doig, A. J.; Hecht, L.; Barron, L. D. *J. Mol. Biol.* **2000**, *301*, 553.
(120) Asher, S. A.; Mikhonin, A. V.; Bykov, S. B. *J. Am. Chem. Soc.* **2004**, *126*, 8433.
(121) Adzhubei, A. A.; Sternberg, M. J. E. *J. Mol. Biol.* **1993**, *229*, 472.
(122) Chen, K.; Liu, Z.; Kallenbach, N. R. *Proc. Natl. Acad. Sci. U.S.A.* **2004**, *101*, 15352.
(123) Garcia, A. E. *Polymer* **2004**, *45*, 669.
(124) Pappu, R. V.; Rose, G. D. *Protein Sci.* **2002**, *11*, 2437.
(125) Bochicchio, B.; Tamburro, A. M. *Chirality* **2002**, *14*, 782.
(126) Woody, R. W. *Adv. Biophys. Chem.* **1992**, *2*, 37.
(127) Fleming, P. J.; Fitzkee, N. C.; Mezei, M.; Srinivasan, R.; Rose, G. D. *Protein Sci.* **2005**, *14*, 111.
(128) Eisenhaber, F.; Adzhubei, A. A.; Eisenmenger, F.; Esipova, N. G. *Biofizika* **1992**, *37*, 62.
(129) Bochicchio, B.; Pepe, A.; Tamburro, A. M. *Chirality* **2005**, *17*, 364.
(130) Blanch, E. W.; Gill, A. C.; Rhie, A. G. O.; Hope, J.; Hecht, L.; Nielsen, K.; Barron, L. D. *J. Mol. Biol.* **2004**, *343*, 467.
(131) Blanch, E. W.; Kasarda, D. D.; Hecht, L.; Nielsen, K.; Barron, L. D. *Biochemistry* **2003**, *42*, 5665.
(132) Blanch, E. W.; Robinson, D. J.; Hecht, L.; Barron, L. D. *J. Gen. Virol.* **2001**, *82*, 1499.
(133) Shi, Z.; Olson, C. A.; Rose, G. D.; Baldwin, R. L.; Kallenbach, N. R. *Proc. Natl. Acad. Sci. U.S.A.* **2002**, *99*, 9190.
(134) McColl, I. H.; Blanch, E. W.; Hecht, L.; Kallenbach, N. R.; Barron, L. D. *J. Am. Chem. Soc.* **2004**, *126*, 5076.
(135) Mikhonin, A. V.; Myshakina, N. S.; Bykov, S. V.; Asher, S. A. *J. Am. Chem. Soc.* **2005**, *127*, 7712.
(136) Gokce, I.; Woody, R. W.; Anderluh, G.; Lakey, J. H. *J. Am. Chem. Soc.* **2005**, *127*, 9700.
(137) Kim, Y. S.; Wang, J.; Hochstrasser, R. M. *J. Phys. Chem. B* **2005**, *109*, 7511.
(138) Woutersen, S.; Hamm, P. *J. Phys. Chem. B* **2000**, *104*, 11316.
(139) Rucker, A. L.; Creamer, T. P. *Protein Sci.* **2002**, *11*, 980.

(140) Makowska, J.; Rodziewicz-Motowidlo, S.; Baginska, K.; Vila, J. A.; Liwo, A.; Chmurzynski, L.; Scheraga, H. A. *Proc. Natl. Acad. Sci. U.S.A.* **2006**, *103*, 1744.
(141) Shi, Z.; Chen, K.; Liu, Z.; Kallenbach, N. R. *Chem. Rev.* **2006**, *106*, 1877.
(142) Shi, Z.; Woody, R. W.; Kallenbach, N. R. *Adv. Protein Chem.* **2002**, *62*, 163.
(143) Chi, Z.; Chen, X. G.; Holtz, J. S. W.; Asher, S. A. *Biochemistry* **1998**, *37*, 2854.
(144) Asher, S. A.; Ianoul, A.; Mix, G.; Boyden, M. N.; Karnoup, A.; Diem, M.; Schweitzer-Stenner, R. *J. Am. Chem. Soc.* **2001**, *123*, 11775.
(145) Mikhonin, A. V.; Ahmed, Z.; Ianoul, A.; Asher., S. A. *J. Phys. Chem. B* **2004**, *108*, 19020.
(146) Chi, Z.; Asher, S. A. *Biochemistry* **1998**, *37*, 2865.
(147) Chi, Z.; Asher, S. A. *Biochemistry* **1999**, *38*, 8196.
(148) Shashilov, V. A.; Xu, M.; Ermolenkov, V. V.; Lednev, I. K. *J. Quant. Spectrosc. Radiat. Transfer* **2006**, *102*, 46.
(149) Xu, M.; Ermolenkov, V. V.; He, W.; Uversky, V. N.; Fredriksen, L.; Lednev, I. K. *Biopolymers* **2005**, *79*, 58.
(150) Copeland, R. A.; Spiro, T. G. *Biochemistry* **1987**, *26*, 2134.
(151) JiJi, R. D.; Balakrishnan, G.; Hu, Y.; Spiro, T. G. *Biochemistry* **2006**, *45*, 34.
(152) Spiro, T. G.; Smulevich, G.; Su, C. *Biochemistry* **1990**, *29*, 4497.
(153) Lednev, I. K.; Ermolenkov, V. V.; He, W.; Xu, M. *Anal. Bioanal. Chem.* **2005**, *381*, 431.
(154) Wang, Y.; Purrello, R.; Jordan, T.; Spiro, T. G. *J. Am. Chem. Soc.* **1991**, *113*, 6359.
(155) Topilina, N. I.; Higashiya, S.; Rana, N.; Ermolenkov, V. V.; Kossow, C.; Carlsen, A.; Ngo, S. C.; Wells, C. C.; Eisenbraun, E. T.; Dunn, K. A.; Lednev, I. K.; Geer, R. E.; Kaloyeros, A. E.; Welch, J. T. *Biomacromolecules* **2006**, *7*, 1104.
(156) Ahmed, Z.; Asher, S. A. *Biochemistry* **2006**, *45*, 9068.
(157) Ahmed, Z.; Beta, I. A.; Mikhonin, A. V.; Asher, S. A. *J. Am. Chem. Soc.* **2005**, *127*, 10943.
(158) Miick, S. M.; Martinez, G. V.; Fiori, W. R.; Todd, A. P.; Millhauser, G. L. *Nature* **1992**, *359*, 653.
(159) Fiori, W. R.; Miick, S. M.; Millhauser, G. L. *Biochemistry* **1993**, *32*, 11957.
(160) Millhauser, G. L. *Biochemistry* **1995**, *34*, 3873.
(161) Martinez, G.; Millhauser, G. *J. Struct. Biol.* **1995**, *114*, 23.
(162) Millhauser, G. L.; Stenland, C. J.; Bolin, K. A.; van de Ven, F. J. M. *J. Biomol. NMR* **1996**, *7*, 331.
(163) Hanson, P.; Martinez, G.; Millhauser, G.; Formaggio, F.; Crisma, M.; Toniolo, C.; Vita, C. *J. Am. Chem. Soc.* **1996**, *118*, 271.
(164) Millhauser, G. L.; Stenland, C. J.; Hanson, P.; Bolin, K. A.; van de Ven, F. J. M. *J. Mol. Biol.* **1997**, *267*, 963.
(165) Hanson, P.; Anderson, D. J.; Martinez, G.; Millhauser, G.; Formaggio, F.; Crisma, M.; Toniolo, C.; Vita, C. *Mol. Phys.* **1998**, *95*, 957.
(166) Armen, R.; Alonso, D. O. V.; Daggett, V. *Protein Sci.* **2003**, *12*, 1145.
(167) Long, H. W.; Tycko, R. *J. Am. Chem. Soc.* **1998**, *120*, 7039.
(168) Topol, I. A.; Burt, S. K.; Deretey, E.; Tang, T.-H.; Perczel, A.; Rashin, A.; Csizmadia, I. G. *J. Am. Chem. Soc.* **2001**, *123*, 6054.
(169) Podtelezhnikov, A. A.; Wild, D. L. *Proteins* **2005**, *61*, 94.
(170) Han, W.-G.; Elstner, M.; Jalkanen, K. J.; Frauenheim, T.; Suhai, S. *Int. J. Quantum Chem.* **2000**, *78*, 459.
(171) Mikhonin, A. V.; Asher, S. A. *J. Am. Chem. Soc.* **2006**, *128*, 13789.
(172) Lee, K.-H.; Benson, D. R.; Kuczera, K. *Biochemistry* **2000**, *39*, 13737.
(173) Mahadevan, J.; Lee, K.-H.; Kuczera, K. *J. Phys. Chem. B* **2001**, *105*, 1863.
(174) Feig, M.; MacKerell, A. D. Jr.; Brooks, C. L. III. *J. Phys. Chem. B* **2003**, *107*, 2831.
(175) Bykov, S. V.; Lednev, I. K.; Ianoul, A.; Mikhonin, A. V.; Munro, C. H.; Asher, S. A. *Appl. Spectrosc.* **2005**, *59*, 1541.
(176) Walrafen, G. E.; Fisher, M. R.; Hokmabadi, M. S.; Yang, W. H. *J. Chem. Phys.* **1986**, *85*, 6970.
(177) Risovic, D.; Furic, K. *J. Raman Spectrosc.* **2005**, *36*, 771.
(178) Mikhonin, A. V.; Asher, S. A. *J. Phys. Chem. B* **2005**, *109*, 3047.
(179) Mikhonin, A. V.; Bykov, S. V.; Myshakina, N. S.; Asher, S. A. *J. Phys. Chem. B* **2006**, *110*, 1928.
(180) Nelles, O. *Nonlinear System Identification*; Springer: New York, 2001.
(181) Dennis, J. E.; Schnabel, R. B. *Numerical Methods for Unconstrained Optimization and Nonlinear Equation*; Prentice Hall: New York, 1983.
(182) Budil, D. E.; Lee, S.; Saxena, S.; Freed, J. H. *J. Magn. Reson., Ser. A* **1996**, *120*, 155.
(183) Gleser, L. J. *Stat. Sci.* **1998**, *13*, 277.
(184) *Grams/32AI User's Guide*; Galactic Industries Corporation, 2001.
(185) Wadsworth, H. M. *Handbook of Statistical Methods for Engineers and Scientists*; McGraw-Hill: New York, 1990.
(186) Lee, S.-H.; Krimm, S. *Biopolymers* **1998**, *46*, 283.
(187) Pimenov, K. V.; Bykov, S. V.; Mikhonin, A. V.; Asher, S. A. *J. Am. Chem. Soc.* **2005**, *127*, 2840.
(188) Copeland, R. A.; Spiro, T. G. *J. Am. Chem. Soc.* **1986**, *108*, 1281.
(189) Tanaka, M.; Tanaka, J. *Mol. Phys.* **1970**, *19*, 889.
(190) Rosenheck, K.; Doty, P. *Proc. Natl. Acad. Sci. U.S.A.* **1961**, *47*, 1775.
(191) Moffit, W. *Proc. Natl. Acad. Sci. U.S.A.* **1956**, *42*, 736.
(192) Schellman, J. A.; Becktel, W. J. *Biopolymers* **1983**, *22*, 171.
(193) Momii, R. K.; Urry, D. W. *Macromolecules* **1968**, *1*, 372.
(194) Painter, P. C.; Koenig, J. L. *Biopolymers* **1976**, *15*, 241.
(195) Weissbluth, M. *Q. Rev. Biophys.* **1971**, *4*, 1.
(196) Rhodes, W.; Barnes, D. G. *J. Chim. Phys. PCB* **1968**, *65*, 78.
(197) McLachlan, A. D.; Ball, M. A. *Mol. Phys.* **1964**, *8*, 581.
(198) Cartailler, J.-P.; Luecke, H. *Structure* **2004**, *12*, 133.
(199) Sundaralingam, M.; Sekharudu, Y. C. *Science* **1989**, *244*, 1333.
(200) Vila, J. A.; Ripoll, D. R.; Scheraga, H. A. *Proc. Natl. Acad. Sci. U.S.A.* **2000**, *97*, 13075.